



**NTNU – Trondheim**  
Norwegian University of  
Science and Technology

# CFD Analysis of a Pelton Turbine

**Lorentz Fjellanger Barstad**

Master of Science in Product Design and Manufacturing

Submission date: June 2012

Supervisor: Ole Gunnar Dahlhaug, EPT

Norwegian University of Science and Technology  
Department of Energy and Process Engineering



EPT-M-2012-28

**MASTER THESIS**

for

Lorentz Fjellanger Barstad

Spring 2012

**CFD-analysis of a Pelton turbine***CFD-analyse av en Pelton turbin***Background**

Among Norway's 1050 hydro power plants, 30% are installed with Pelton turbines. Most of the large Pelton turbines are more than 30 years old and therefore power plant owners are looking for refurbishments. Since each Pelton turbine is unique, the turbine designer has to design new Pelton turbine runners every time a new or replaced turbine is being developed.

The development of Pelton turbines has not changed much during the last three decades. However, the introduction of numerical tools has changed the design engineer's procedures in the process of new Pelton turbine designs. This work will look in to the CFD-analysis of the flow in the Pelton runner bucket.

**Objective**

CFD-analysis of the flow in a Pelton turbine bucket

**The following tasks are to be considered:**

1. Literature survey
  - a. The student must complete a literature survey on state of the art within CFD-analysis of the flow in the Pelton turbine bucket.
2. Software knowledge
  - a. Get familiar with the CFD-tool; Ansys/CFX
3. Parametric study of a Pelton turbine design
  - a. Get familiar with the design program for Pelton Turbines developed by Bjørn Winther Solemslie
  - b. Change the design of the turbine bucket
4. Carry out a CFD-analysis for at least three different turbine bucket designs
5. If there are time available and model test is available a comparison of the CFD-analysis and experimental work will be carried out

Within 14 days of receiving the written text on the master thesis, the candidate shall submit a research plan for his project to the department.

When the thesis is evaluated, emphasis is put on processing of the results, and that they are presented in tabular and/or graphic form in a clear manner, and that they are analyzed carefully.

The thesis should be formulated as a research report with summary both in English and Norwegian, conclusion, literature references, table of contents etc. During the preparation of the text, the candidate should make an effort to produce a well-structured and easily readable report. In order to ease the evaluation of the thesis, it is important that the cross-references are correct. In the making of the report, strong emphasis should be placed on both a thorough discussion of the results and an orderly presentation.

The candidate is requested to initiate and keep close contact with his/her academic supervisor(s) throughout the working period. The candidate must follow the rules and regulations of NTNU as well as passive directions given by the Department of Energy and Process Engineering.

Risk assessment of the candidate's work shall be carried out according to the department's procedures. The risk assessment must be documented and included as part of the final report. Events related to the candidate's work adversely affecting the health, safety or security, must be documented and included as part of the final report.

Pursuant to "Regulations concerning the supplementary provisions to the technology study program/Master of Science" at NTNU §20, the Department reserves the permission to utilize all the results and data for teaching and research purposes as well as in future publications.

The final report is to be submitted digitally in DAIM. An executive summary of the thesis including title, student's name, supervisor's name, year, department name, and NTNU's logo and name, shall be submitted to the department as a separate pdf file. Based on an agreement with the supervisor, the final report and other material and documents may be given to the supervisor in digital format.

Department of Energy and Process Engineering, 10. January 2012



Olav Bolland  
Department Head



Ole Gunnar Dahlhaug  
Academic Supervisor

Research Advisors: Bjørn Winther Solemslie, PhD-student

# Abstract

A Pelton design software is currently being developed at the Waterpower laboratory at NTNU. The motivation behind this software is to streamline the parametric design process for Pelton turbines. A numerical flow model is a cornerstone in this application, but the lack of a bucket geometry and model runner has prevented the development of such a model. DynaVec, a turbine producer who specializes on sediment erosion and corrosion problems, offered to help by providing a bucket geometry and a model runner.

The objective of this Master's thesis was to develop and validate a CFD model that predicts the torque applied to a non-stationary Pelton bucket, subject to a high-speed water jet. The numerical model was based on a method proposed by DynaVec, and the bucket geometry used in the simulations was identical (1:1) to the model runner.

Numerous simulations were conducted, testing mesh dependency and different operational points (e.g. head). Mesh independence occurred at approximately 4.5 million elements. Furthermore, simulations of varying heads showed that the model may be independent of the head (40-80m), but this was not verified properly.

Experiments showed that the numerical prediction was fairly accurate. A comparison of the numerical and experimental measurements showed that the CFD model over-predicts the torque by approximately 1.5%. This prediction was validated for the specific geometry used in the simulations, and a head of 75m.

Overall, the results suggest that the numerical model is promising as a parametric design tool, but further development is required to obtain a true validation of the model.

Task three and four were changed in agreement with Ole Gunnar Dahlhaug, because Solemslie's design program was delayed. In essence, the parametric study proceeded in favor of the development of a CFD model. To ensure that this work would benefit future research, especially students at the Waterpower laboratory, a detailed procedure for the CAD modeling, meshing and physical setup was included in the Appendix.



# Sammendrag

En programvare for parametrisk design av Pelton turbiner utvikles fortiden på Vannkraftlaboratoriet ved NTNU. Målet med dette programmet er å effektivisere designprosessen og dermed tilrettelegge for flere designstudier. En numerisk strømningsmodell utgjør en viktig del av en slik programvare, men mangelen på en skovlgeometri og et tilhørende løpehjul har til nå, utsatt dette prosjektet. Turbinprodusenten DynaVec, som spesialiserer seg på sanderosjon og korrosjonsproblemer, kunne hjelpe med akkurat dette. En skovlgeometri og modellturbin ble gitt til disposisjon.

Oppgavens hovedmål var å utvikle og validere en CFD-modell som predikrer momentet en høyhastighets vannstråle tilfører en roterende Pelton skovl. Den numeriske modellen er basert på en metode foreslått av DynaVec. Skovl geometrien som ble brukt i simuleringene var identisk (1:1) med geometrien brukt på løpehjulet.

Flere simuleringer testet mesh-uavhengighet og innvirkningen ulike fallhøyder har på modellen. Mesh-uavhengighet oppstod ved ca. 4.5 millioner elementer. Videre viste fallhøyde simuleringene at modellen er forholdsvis uavhengig av fallhøyde (40-80m), men dette ble ikke verifisert skikkelig.

Eksperimentelle målinger viste at den numeriske prediksjonen av momentet var tilfredsstillende. CFD-modellen ble validert for en over-prediksjon av momentet på ca. 1.5%. Validiteten, derimot, gjelder kun for den spesifikke geometrien brukt i denne oppgaven og ved en fallhøyde på 75m.

Oppsummert virker CFD-modellen lovende som en del av et parametrisk designverktøy for Pelton turbiner, men videre utvikling og testing er nødvendig for å optimalisere modellen.

Oppgave tre og fire ble forandret til å omhandle utvikling av en CFD-modell, etter avtale med Ole Gunnar Dahlhaug. For at arbeidet som er blitt gjort i forbindelse med denne modellen skal kunne brukes videre, spesielt av studenter ved Vannkraftlaboratoriet, er denne blitt presentert grundig. En detaljert prosedyre for CAD-modellering, meshing og fysisk modell finnes som vedlegg til denne oppgaven.



# Preface

This Master's thesis was written at the Waterpower laboratory at the Norwegian University of Science and Technology.

During the course of this semester my work has focused on conducting numerous CFD simulations, in contrast to the experimental work last semester. I am very grateful for this opportunity, because it has allowed me to experience both the theoretical and practical aspects of a technical project.

Doctoral candidate, Bjørn Winther Solemslie, has filled the role as my mentor in the past year. His enthusiasm and positive attitude has without doubt, inspired my work. DynaVec, a mentor and contributor to the CFD analysis, also deserves my gratitude. Their involvement made this thesis possible, and I hope my work will be beneficial for them as well as for NTNU. I also want to thank my supervisor, Ole Gunnar Dahlhaug. He has been a great source of inspiration, and was responsible for the involvement of DynaVec. Last but not least, I want to thank the rest of the staff and students at the Waterpower laboratory, for creating an excellent learning environment.

I also would like to point out that the openness and close collaboration between master students, doctoral candidates and professors at the laboratory has been a great motivator in terms of learning and the will to succeed.

Now, I embark upon the working life, but I will never forget my year at the Waterpower laboratory.



---

Lorentz Fjellanger Barstad  
Trondheim, June 9, 2012



# Contents

<b>Abstract</b>	<b>i</b>
<b>Abstract in Norwegian</b>	<b>iii</b>
<b>Preface</b>	<b>v</b>
<b>List of Figures</b>	<b>xii</b>
<b>List of Tables</b>	<b>xiii</b>
<b>Nomenclature</b>	<b>xvi</b>
<b>Introduction</b>	<b>1</b>
<b>1 Previous Work</b>	<b>3</b>
1.1 M. Hana . . . . .	3
1.2 G. Berntsen . . . . .	4
1.3 A. Perrig . . . . .	5
1.4 L. Klemetsen . . . . .	5
1.5 DynaVec AS . . . . .	7
<b>2 Theory</b>	<b>9</b>
2.1 The Pelton Turbine . . . . .	9
2.1.1 Energy conversion . . . . .	9
2.1.2 Maximum Water Jet Velocity . . . . .	11
2.1.3 Optimal Rotational Speed . . . . .	12
2.2 Computational Fluid Dynamics . . . . .	13
2.2.1 Review of CFD-codes . . . . .	13
2.2.2 Turbulence Modeling . . . . .	14
2.2.3 Multiphase Modeling . . . . .	15
2.2.4 Meshing . . . . .	16
2.2.5 Verification & Validation . . . . .	18
<b>3 CFD Analysis</b>	<b>19</b>
3.1 Objective and Challenges . . . . .	19

3.2	Methodology . . . . .	19
3.3	Workflow . . . . .	21
3.3.1	CAD Modeling with ANSYS DesignModeler . . . . .	22
3.3.2	Meshing with ANSYS Meshing . . . . .	23
3.3.3	Physical Setup with ANSYS Pre . . . . .	23
3.3.4	Post-Processing . . . . .	27
3.4	Simulations . . . . .	28
3.4.1	Surface Tension Coefficient . . . . .	28
3.4.2	Mesh Dependency . . . . .	29
3.4.3	Head . . . . .	29
3.5	Results . . . . .	31
3.6	Discussion and Verification . . . . .	36
3.6.1	Mesh Dependency . . . . .	37
3.6.2	Convergence and Stability . . . . .	37
3.6.3	Flow Visualization . . . . .	38
<b>4</b>	<b>Validation of the CFD Model</b>	<b>41</b>
4.1	Experiments . . . . .	41
4.1.1	Instrumentation . . . . .	41
4.1.2	Test Procedure . . . . .	42
4.1.3	Uncertainty . . . . .	43
4.2	Results . . . . .	44
4.3	Discussion . . . . .	47
4.3.1	Uncertainty of Experimental Results . . . . .	47
4.3.2	Hydraulic Efficiency . . . . .	47
4.3.3	Validity of the CFD Model . . . . .	47
<b>5</b>	<b>Conclusion and Further Work</b>	<b>49</b>
<b>Bibliography</b>		<b>51</b>
<b>Appendices</b>		<b>55</b>
<b>A</b>	<b>CFD</b>	<b>55</b>
A.1	Fundamental Equations . . . . .	55
A.2	RANS Turbulence Modeling . . . . .	56
<b>B</b>	<b>Uncertainty in Pelton Model Tests</b>	<b>59</b>
B.1	Torque . . . . .	59
B.1.1	Systematic Errors . . . . .	59
B.1.2	Random Errors . . . . .	60
B.1.3	Total Uncertainty . . . . .	60
B.2	Total Torque . . . . .	61
<b>C</b>	<b>ANSYS DesignModeler Workflow</b>	<b>63</b>
C.1	Stationary domain . . . . .	63
C.2	Rotating domain . . . . .	72

<b>D ANSYS Meshing Workflow</b>	<b>75</b>
D.1 Stationary domain . . . . .	75
D.2 Rotating domain . . . . .	77
<b>E ANSYS Pre Detailed Setup</b>	<b>79</b>
E.1 Expressions . . . . .	79
E.2 Analysis Type . . . . .	80
E.3 Domains . . . . .	80
E.4 Boundary Conditions . . . . .	81
E.5 Interfaces . . . . .	82
E.6 Solver . . . . .	83
E.6.1 Solver Units . . . . .	83
E.6.2 Solver Control . . . . .	83
E.6.3 Output Control . . . . .	83
<b>F MATLAB Post-Processing</b>	<b>85</b>
F.1 Total Torque Matrix . . . . .	85
F.2 File: CreateT.m . . . . .	87



# List of Figures

1.1	Normalized total pressure versus normalized radial distance. [1]	4
1.2	Details of Perrig's computational grid. [2]	5
1.3	Velocity boundary conditions at the inlet. [3]	6
1.4	Definition of the velocity inlet in A. CFX. [3]	6
2.1	Schematics of a Pelton turbine with 6 nozzles. [4]	10
2.2	Bucket geometry [2]	10
2.3	Energy conversion in a Pelton turbine runner. [5]	11
2.4	Pelton turbine velocity vectors. [5]	12
2.5	Steady and unsteady turbulent flow. [6]	15
2.6	Mesh cell/element types in A. Meshing. [7]	17
2.7	Cell-centered vs. vertex-centered. [7]	17
2.8	Mesh quality for A. CFX. [7]	18
3.1	Example sketch based on DynaVec's CFD Setup.	20
3.2	ANSYS Workbench overview of a simulation.	21
3.3	Assembly of the rotating and stationary domain.	22
3.4	Mesh	24
3.5	Total torque on runner (red) from duplic	27
3.6	Mass and momentum residuals for MD8 ( $\sigma_2$ )	32
3.7	Middle bucket torque for simulations with	32
3.8	Comparison of the middle bucket torque with	33
3.9	Mesh dependency results.	34
3.10	Volume fractions in frame 9 (Figure 3.11).	34
3.11	Flow visualization for the MD8 simulation.	35
4.1	NTNU Pelton model rig. [1]	42
4.2	Total torque $\tau_{tot}$ deviation between mesh depende	44
4.3	Total torque $\tau_{tot}$ deviation between head simula	45
4.4	MD6 ( $\sigma_2$ ) simulation vs. experiment (E4)	46
C.1	Sketch: Stator	64
C.2	Sketch: Nozzle1	64
C.3	Sketch: Nozzle2	65

C.4	Sketch: JetSlice1 and JetSlice2 . . . . .	65
C.5	Sketch: JetCore . . . . .	66
C.6	Overview of the 4 slice surfaces in Step 10. . . . .	68
C.7	Step 10 after slicing. . . . .	69
C.8	Jet domain after slicing. Note that the jet core consists of three bodies. . . . .	70
C.9	Named Selections: Stationary domain . . . . .	71
C.10	Sketch: RotatingDomain . . . . .	72
C.11	Sketch: BoI1 . . . . .	73
C.12	Named Selections: Rotating domain . . . . .	74
D.1	Area numbering . . . . .	76
D.2	Rotating mesh . . . . .	77

# List of Tables

2.1	Mesh quality thresholds for A. CFX. [8]	18
3.1	Overview of the basic setup used for all simulations.	28
3.2	Overview of the mesh dependency tests.	30
3.3	Mesh characteristics.	30
3.4	Overview of the Head tests.	31
3.5	Overview of the simulation results.	31
4.1	Overview of the experiments.	43
4.2	Torque uncertainties at varying heads.	44
A.1	RANS turbulence models. [3]	57
B.1	Constant systematic uncertainties provided by Reinertsen. [9]	60
E.1	Expressions defined in ANSYS Pre	80



# Nomenclature

$B$	bucket width, $m$	$\theta$	angular position, $^{\circ}$
$D$	runner diameter, $m$	$\varphi$	friction coefficient
$d_s$	jet diameter, $m$		
$f_z$	bucket frequency, $s^{-1}$		
$g$	acceleration of gravity, $m/s^2$		
$H$	head, $mWc$		
$h$	pressure head, $mWc$		
$L$	length, $m$		
$n$	bucket duplicates (Sec. 3.3.4)		
$n$	rotational speed, $rpm$		
$Q$	volume flow, $m^3/s$		
$t$	time, $s$		
$\mathbf{V}$	Eulerian velocity field		
$R_e$	Reynolds number		
$v_f$	volume fraction		
$Z$	number of buckets		
$u$	peripheral velocity, $m/s$		
$c$	absolute velocity, $m/s$		
$w$	relative velocity, $m/s$		
$e_X$	absolute uncertainty of X		
$f_X$	relative uncertainty of X		
$S_X$	standard deviation of X		
<b>Greek Symbols</b>			
$\eta$	efficiency		
$\nu$	kinematic viscosity, $m^2/s$		
$\omega$	angular velocity, $s^{-1}$		
$\pi$	constant		
$\rho$	density, $kg/m^3$		
$\sigma$	surface tension coeff., $N/m$		
$\tau$	torque, $Nm$		
<b>Subscripts</b>			
1	inlet runner, ( $\sigma$ , Chapter 3-5)		
1*	inlet nozzle		
2	outlet runner ( $\sigma$ , Chapter 3-5)		
3	tailwater		
<i>abs</i>	absolute		
<i>e</i>	effective		
<i>fr</i>	friction		
<i>gen</i>	generator		
<i>h</i>	hydraulic		
<i>r</i>	random		
<i>s</i>	systematic		
<i>tot</i>	total		
<i>u</i>	velocity component u-direction		
<b>Abbreviations</b>			
<i>CFD</i>	Computational Fluid Dynamics		
<i>SST</i>	Shear Stress Transport		
<i>CAD</i>	Computer Aided Design		
<i>CFX</i>	CFD code by ANSYS		
<i>GUI</i>	Graphical User Interface		
<i>IEC</i>	International Electrotechnical Commission		
<i>RMS</i>	Root Mean Square		
<i>SPH</i>	Smoothed-Particle Hydrodynamics		
<i>VOF</i>	Volume of Fluid		



# Introduction

Hydropower is a renewable energy resource that can produce electricity without using fossil fuels. The environmental consequences of hydropower are related to the disturbances of natural ecosystems due to damming, lowering of the water level, altered water flow and new infrastructure. Norway is in an unique position due to the fact that a large part of the domestic energy consumption and power demanding industries, are fueled by electricity. Maintaining and developing the hydropower industry is without a doubt crucial, especially in this day and age where climate changes strongly encourage the use of green technologies.

The Pelton turbine absorbs energy from a high-speed water jet and is characterized by high heads and small volume flows. Even though this is a well established turbine technology, there are many unanswered questions regarding design and optimization. Thus, further development is still relevant today.

In the autumn of 2010 MSc student, Kristine Gjøsaeter, began the process of developing a Francis turbine design software called *Khoj*. [10] Peter Joachim Gogstad continued the development of *Khoj* with his MSc thesis. [11] Hopes are that more people will be able to conduct experiments, and participate in the development of the Francis turbine.

*Khoj* is a MATLAB application with a user friendly GUI that produces a geometry output readable by Pro/ENGINEER and ANSYS CFX (A. CFX) for mechanical design and hydraulic analysis, respectively. A similar software has been requested for the Pelton turbine, but the lack of an open Pelton bucket design has prevented this development.

Doctoral candidate, Bjørn Winther Solemslie, is currently in the process of designing a new reference Pelton turbine on behalf of NTNU. A new design provides the opportunity to develop a Pelton design software, such as *Khoj*. This thesis will initiate the development of a Pelton CFD model, that will be a part of a Pelton design software in the future.

Numerous CFD analyses on the flow in Pelton buckets have previously been carried out, but apparently a transient analysis of a free surface water jet interacting with rotating Pelton buckets, has not yet been attempted at NTNU. The main objective of this thesis will be to perform the latter, and validate the torque measurement

produced by the CFD model. To ensure that this work will benefit future students at the Waterpower laboratory, a detailed procedure for CAD modeling, meshing and A. CFX setup will also be created.

DynaVec, a company based in Trondheim, has experience with CFD analyses on Pelton turbines. They offered their assistance and could provide a CAD model for a bucket used in a model turbine. This turbine will be tested experimentally in the Waterpower laboratory at NTNU, which will be a crucial part of the validation of the CFD model.

# Chapter 1

## Previous Work

Previous research on Pelton turbines consist mainly of analytical, numerical and experimental studies. This section will briefly highlight the research of interest to this thesis.

Early on, professor H. Brekke analytically developed a method to reconstruct the path of water particles on their relative momentum equations in the bucket. [3] Brekke [12] based his work on a graphical particle trace method developed by Henrik Christie in 1918. Hana [13] investigated and partially improved this method.

The numerical analyses of the free surface flow in a Pelton bucket have generally utilized commercial CFD tools with mesh-based solvers. Another approach is the mesh-free Lagrangian method which completely eliminates the difficulties with traditional mesh-based techniques. Smoothed-particle hydrodynamics (SPH) is a promising Lagrangian method, but it is still in an early developing stage with few published studies, which need to be correctly validated [2].

The experimental studies generally involve steady and transient pressure measurements, flow visualization and water film thickness measurements.

### 1.1 M. Hana

Morten Hana's PhD thesis "Numerical analysis of non-stationary free surface flow in a Pelton bucket" [13], published in 1999, was the first study of its kind [3]. With the help of three commercial CFD-codes (RIPPLE, Flow-3D and CFX-4), Hana ran both simplified 2D-simulations and transient 3D-simulations of the free surface flow in a Pelton bucket. Three problem areas were highlighted: the free surface, complex geometry and the relative motion of the jet and the buckets. The performance of the different codes and methods were evaluated, and Hana

concluded that numerical calculations showed promising results and can replace the graphical method when numerical calculations has been verified.

## 1.2 G. Berntsen

In 2003, Gotfred Severin Berntsen published his PhD thesis "Numerical analysis of the two-phase Pelton jet flow using a single-phase model and analytical discussions of the Pelton jet surface break-up phenomenon" [1]. With this thesis Berntsen develops a single-phase CFD model called virtual interphase method (VIP) that can be used to calculate any free surface jet where a high density ratio is present.

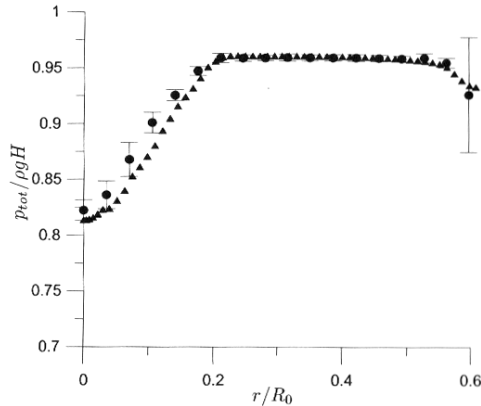


Figure 1.1: Normalized total pressure versus normalized radial distance. Dots denote measured values and triangles denote numerical values. The similarities are characterized as good. [1]

The VIP model is an alternative to the traditional and commonly used VOF (Volume of Fluid) model. The main difference between the two is that the VIP model calculates a necessary grid adaption between iteration steps resulting in a remake of the computational grid for every iteration step. Through experiments, Berntsen shows that the modeling issues in the VOF approach is eliminated with the VIP model. Jet surface ripples and jet-break up is discussed using analytical methods.

With Berntsen's results, all flow features are captured well up to about 2 nozzle diameters away from the nozzle. The results are still accurate in some areas further down stream, but Berntsen concludes that the model needs further development in order to properly account for the inevitable jet break-up at large distances from the nozzle.

Berntsen's VIP model is something that could be useful and worth investigating further.

### 1.3 A. Perrig

In 2007, Alexandre Perrig publish his comprehensive PhD thesis "Hydrodynamics of the Free Surface Flow in Pelton Turbine Buckets" [2]. Perrig studied the flow in the buckets with 4 experimental and numerical approaches: (i) Unsteady onboard wall pressure measurements. (ii) High-speed flow visualizations. (iii) Onboard water film thickness measurements. (iv) CFD simulations. He compared the 2-Phase Homogeneous Model and the 2-Fluid Model, and concluded that the latter one was the most accurate. However, the accuracy of the 2-Phase Homogeneous Model decreases significantly with the successive time steps.

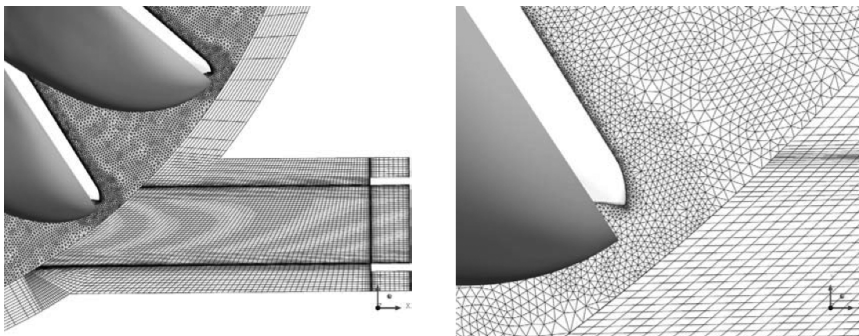


Figure 1.2: Details of Perrig's computational grid. [2]

The 2-Fluid Model is recommended and should be run with a large number of iterations to reach complete convergence. Perrig states that the main drawback associated with the classic CFD approaches is the need for refined meshes in the whole domain, while the region of interest for any give time step only represent a fraction of the domain. As this dramatically increases the computational cost, accurate numerical simulations of a full-scale facility appears highly difficult.

Perrig's work is relevant to this thesis because his numerical CFD simulation setup is very similar to what the author is trying to achieve. Experimentation with the 2-Phase Homogeneous Model and the 2-Fluid Model is also of interest.

### 1.4 L. Klemetsen

To the authors knowledge, the most recent norwegian study of the free surface flow in Pelton turbine buckets is Lars Erik Klemetsen's MSc thesis "An experimental and numerical study of the free surface Pelton bucket flow" [3] published in 2010. Klemetsen investigated a simplification of the free surface flow through a static Pelton turbine bucket. Through experiments the pressure distribution throughout the majority of the flow domain was obtained, as well as the location of the air-water interface. Afterwards, these results were compared with numerical simulations

using two commercial CFD-solvers (Fluent 6.4 and CFX). This comparison showed that the flow problem was practically independent of turbulence modeling and mesh (as long as the grid resolution was kept above a certain lower limit). Gravity, viscosity and surface tension could also be neglected due to the dominance of inertia forces.

The use of mesh adaption algorithms at the water-air interface was an effective improvement and the adjustments made to the velocity profile affected the results the most. Klemetsen suggests the use of a dynamic mesh refinement for transient full cycle simulations of rotating Pelton buckets due to the fact that the water interface would change continuously. Also, a combined calculation of the nozzle and the bucket profile would be a useful extension of his work.

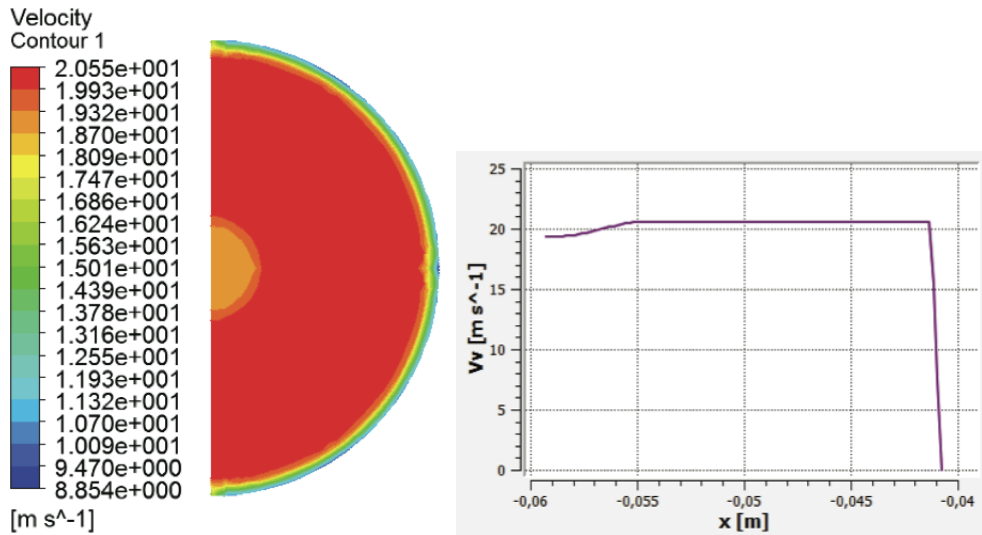


Figure 1.3: Velocity boundary conditions at the inlet. [3]

Figure 1.4: Definition of the velocity inlet in A. CFX. [3]

All tough Klemetsen's work is on a static bucket, it is of great value in order to model the water sheet thickness, inlet boundary conditions and general CFD simulation setup.

## 1.5 DynaVec AS

DynaVec is a company based in Trondheim, which specializes in designing, manufacturing, and installing pumps and turbines for environments with sediment erosion and corrosion problems. Their team consists of highly qualified personnel with many years of experience in hydropower and renewable energy both nationally and internationally. [14] For this thesis, their knowledge and experience of conducting CFD analyses, were especially valuable.



### DynaVec's Contribution

There was no Pelton CAD geometry with experimental data available at NTNU when this thesis was initiated. Because experiments are very important in order to validate a CFD model, it was a requirement to obtain experimental data of a Pelton turbine in combination with a bucket geometry. In the autumn of 2011, DynaVec agreed to share an early stage, noncommercial bucket geometry. This geometry was used in the development of the method of modeling the fluid domain and meshing this domain. Simulations, based on a method proposed by DynaVec, were also conducted in order to see if the CFD model behaved within reason.

In March 2012 DynaVec provided the author with a new bucket geometry of a model turbine, which was tested in the laboratory in April 2012. The CFD analysis presented in this thesis is based on this geometry, and because it is commercial, all results are normalized.



# Chapter 2

## Theory

In this chapter, relevant theory behind the Pelton turbine and CFD is presented. Appendix A presents the fundamental equations of CFD and RANS (Reynolds Averaged Navier- Stokes) turbulence modeling. Section 2.1 is a short version of the theory presented in the authors Project thesis [15].

### 2.1 The Pelton Turbine

The Pelton turbine is a good choice in situations where the volume flow is small relative to the head, typically heads above  $600m$ . The efficiency curve is flat in comparison to the Francis or Kaplan turbine, and the maximum efficiency is lower. The reason for this characteristic is because the turbine is regulated with a multiple number of nozzles, where each nozzle can regulate the volume flow. With this ability in mind, the Pelton turbine is a very good choice if the available head is unpredictable and changes a lot throughout the season. In small power plants ( $<10MW$ ) Pelton turbines are used at heads above  $100m$ , and are especially suitable when there is no reservoir. Figure 2.1 and 2.2 depict the schematic layout and bucket geometry of a Pelton turbine.

#### 2.1.1 Energy conversion

The Pelton turbine is an impulse turbine, which means that the flow energy is completely converted to kinetic energy before conversion in the runner. A direct consequence of this is that there is no pressure difference between the inlet and outlet of the runner. Thus, the mechanical energy transferred to the shaft comes from the impulse forces from the flow alone. The impulse forces are created when a bucket force the flow vectors to change direction. Figure 2.3 demonstrates the

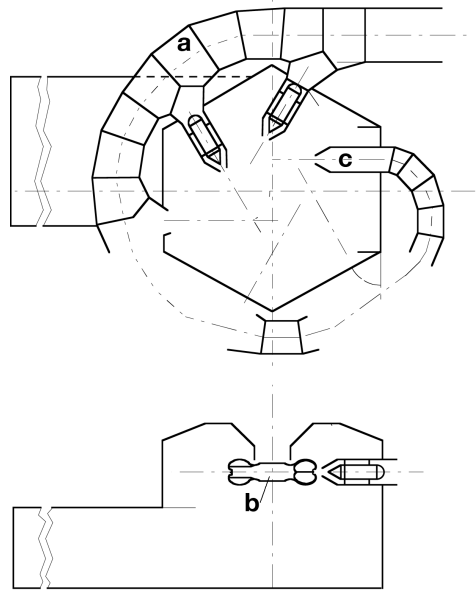


Figure 2.1: Schematics of a Pelton turbine with 6 nozzles. (a) Spiral casing. (b) Runner. (c) Nozzle. [4]

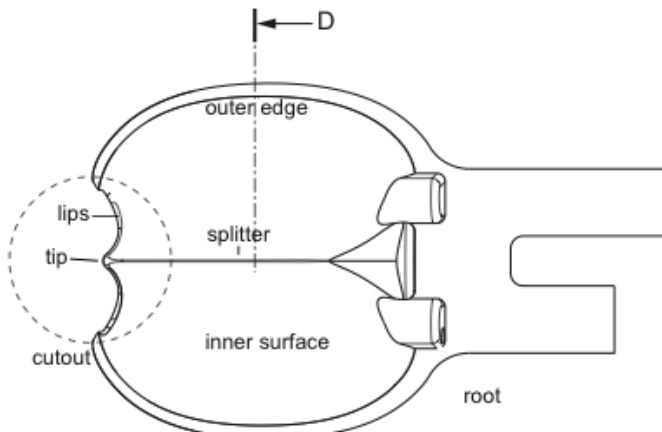


Figure 2.2: Bucket geometry [2]

energy conversion in a Pelton turbine. Step  $1^* \rightarrow 1$  symbolizes the energy conversion in the nozzle. The flow is taken from a state of high pressure and low velocity, to a state of atmospheric pressure and high velocity. Thus, the energy of the flow is completely converted to kinetic energy relative to the mechanical conversion. In step  $1 \rightarrow 2$  almost all the kinetic energy is converted to mechanical energy in the runner. By conducting an energy analysis of a turbomachine runner [16] it can be shown that the specific power  $E_m$  transferred from the water to the runner is a function of the absolute and peripheral velocity at the inlet and outlet of the runner:

$$E_m = c_{u1}u_1 - c_{u2}u_2 \quad (2.1)$$

where  $c_{ui}$  and  $u_i$  is the absolute and peripheral velocity respectively. Dividing  $E_m$  by the total energy available  $E = gH_e$ , result in the Euler equation:

$$\eta_h = \frac{E_m}{E} = \frac{c_{u1}u_1 - c_{u2}u_2}{gH_e} \quad (2.2)$$

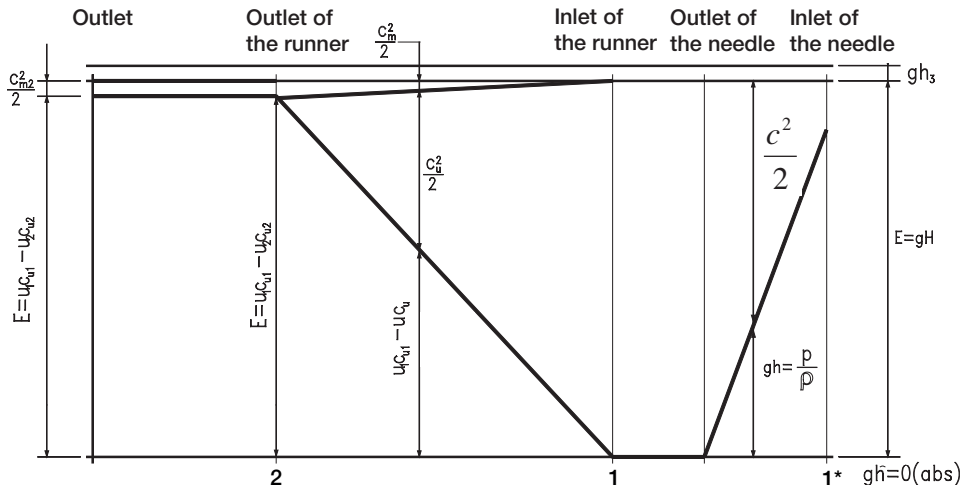


Figure 2.3: Energy conversion in a Pelton turbine runner. [5]

In step 2, the remaining energy can be divided into two components: (1) a small flow velocity  $\frac{c_{m2}^2}{2}$  (relative to the jet) and (2) the potential energy  $gh_3$  of the water relative to the tail-water.

### 2.1.2 Maximum Water Jet Velocity

The Bernoulli equation [17] for steady, incompressible and frictionless flow along a streamline is

$$\frac{p_2 - p_1}{\rho} + \frac{1}{2}(c_2^2 - c_1^2) + g(z_2 - z_1) = 0 \quad (2.3)$$

When losses are neglected the energy is conserved between any two points 1 and 2 on a streamline. The theoretical jet-velocity can be found by evaluating Eq. (2.3) between the distributor inlet and nozzle outlet ( $1^* \rightarrow 1$ ) and solving for  $c_1$ :

$$c_{1,max} = \varphi \sqrt{2g \left( h_{1^*, gauge} + \frac{c_{1^*}^2}{2g} \right)} = \varphi \sqrt{2g H_e} \quad (2.4)$$

Equation (2.3) does not account for the losses in the system. Losses in the nozzle influences the jet-velocity and is corrected by a friction coefficient  $\varphi$  [18].

### 2.1.3 Optimal Rotational Speed

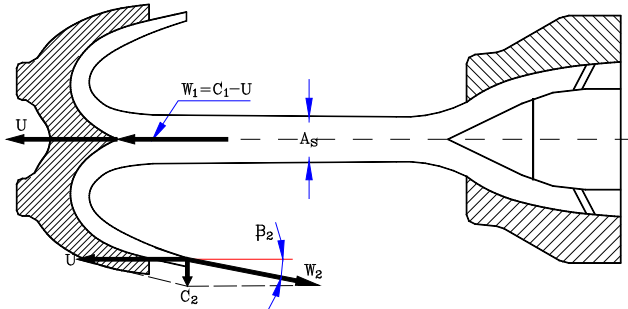


Figure 2.4: Pelton turbine velocity vectors. [5]

The Euler equation (2.2) is very useful when calculating the optimal rotational speed. Figure 2.4 show the relationship between inlet and outlet velocity vectors of a Pelton bucket. If the absolute velocity at the outlet is zero, the water has transferred all its energy (kinetic) to the runner. Setting  $c_{u2} = 0$ , Eq. (2.2) becomes

$$\eta_h = \frac{c_{u1} u_1}{g H_e} \quad (2.5)$$

If one recognizes that  $c_{u1} = c_1$ , implements the expression for maximum water jet-velocity (2.4) and solves Eq. (2.5) for  $u_1$  one obtain the optimal peripheral velocity:

$$u_1 = \frac{\eta_h g H_e}{c_1} = \frac{\eta_h g H_e c_1}{(\varphi \sqrt{2gH_e})^2} = \frac{\eta_h c_1}{2\varphi^2} \quad (2.6)$$

The optimal angular velocity  $\omega$  as a function of  $H_e$ ,  $\eta_h$  and runner diameter  $D$  is

$$\omega = \frac{u_1}{r} = \frac{\eta_h c_1}{\varphi^2 D} = \frac{\eta_h \sqrt{2gH_e}}{\varphi D} \quad (2.7)$$

## 2.2 Computational Fluid Dynamics

Computational Fluid Dynamics (CFD), is a branch within fluid dynamics where numerical methods and algorithms, are used to solve fluid flow problems that are far too complex to solve analytically. The continuously increasing computational power, memory and storage of computers, have made CFD a fast growing tool in recent decades. Analytical solutions to the Navier-Stokes equations exist for only the simplest of flows under ideal conditions. For real flows, a numerical approach must be adopted whereby the equations are replaced by algebraic approximations that can be solved numerically.

A key benefit of CFD, is that a great amount of time and money can be saved concerning experiments. A single analyst equipped with a computer, can replace experiment designing, material costs, measurement equipment, laboratory personnel etc. The purpose of CFD is not to make decisions directly, it works in conjunction with experiments and experience. The results of a CFD analysis should be thoroughly analyzed and validated before the model is accepted. It is also important to understand that the solution is only an approximation due to decretization of the continuos world.

The literature of this section is based mostly on [6], [19], [8] and [3]. In the past few years CFD theory has been covered thoroughly in theses at the Waterpower laboratory and in similar cases (e.g. [3], [2], [20], [21]). Thus, only the essentials relevant to this thesis are presented.

### 2.2.1 Review of CFD-codes

The commercial CFD codes ANSYS CFX and ANSYS Fluent are available at NTNU. The main difference between the two is the way the solvers integrate the flow equations and their solution strategies. CFX uses finite elements (cell vertex numerics) to discretize the domain. Contrarily, Fluent utilizes finite volumes (cell centred numerics). They are both control volume based solvers, which ensure conservation of flow quantities. CFX has only one method to solve the governing equations of motion, a coupled algebraic multi-grid. Fluent differs, as it of-

fers several approaches, such as a pressure-based coupled solver, a fully-segregated pressure-based solver and two density-based solver formulations.

DynaVec has used CFX on Pelton simulations and has achieved satisfying results. Having DynaVec as a reference and mentor, CFX was the most logical choice of solver. Gogstad [11] and Gjøsæter [10] also used CFX on the Khoj project, their work and expertise with CFX is also potentially beneficial in solving the problem.

### 2.2.2 Turbulence Modeling

Smooth, orderly laminar flow is strictly limited to finite values of a critical parameter (Reynolds number, Grashof number, Taylor number, Richardson number). [6] Beyond that, laminar flow is unstable and will evolve to a new flow regime if the critical parameter is high enough. That new regime is dominated by a fluctuating, disorderly motion of called turbulence. A complete analysis and quantification of turbulence will probably never be achieved, due to its complexity and unpredictability by stability theory.

The Reynolds number (2.8) describes the ratio between the inertia and viscous forces in the fluid. Turbulence is characterized by a high Reynolds number which means that the inertia forces are significant compared to the viscous forces. In laminar flow a small perturbation is damped by viscous forces, which is not the case with turbulent flows.

$$Re = \frac{VL}{\nu} = \frac{\text{inertia}}{\text{viscous}} \quad (2.8)$$

There are several different approaches to tackle turbulence. The *Direct numerical simulation* (DNS) method solves the full unsteady Navier-Stokes equations for all turbulence scales and thus uses no model at all. This method is limited to low-turbulent Reynolds numbers and simple flows, due to the high computational cost (the computational grid has to be very fine in order to capture the specific micro scales of the flow). The *Large-eddy simulation* (LES) method is similar to DNS, but differs in the way that it models the smaller sub-grid-scale motions. As with DNS, LES is computationally expensive and primarily used in scientific studies. The third and most used approach is the modeling of the *Reynolds Averaged Navier-Stokes* (RANS) equations. RANS turbulence modeling is far less demanding than the methods above, and the appropriate choice for a Pelton turbine simulation. A DNS or LES simulation is a possible in the future.

### RANS Turbulence Modeling

Turbulent flow could be said to exhibit average characteristics with a time-varying component, when looking at timescales much larger than the timescales of turbulent fluctuations (Fig. 2.5). The RANS equations are the result of the introduction

of averaged and fluctuating quantities to the originally unsteady Navier-Stokes equations. See Appendix A.2 for details. Turbulence models based on the RANS equations are known as Statistical turbulence models due to the statistical averaging procedure.

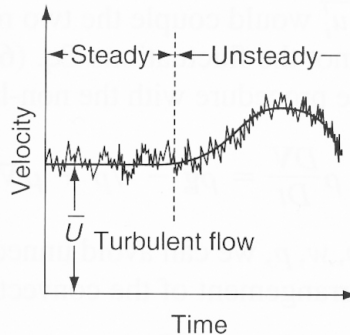


Figure 2.5: Steady and unsteady turbulent flow. [6]

## SST $k-\omega$ model

For prediction of Pelton bucket flow and high accuracy boundary layer simulations, the  $k-\omega$  based SST turbulence model based on the work by Menter [22], is the most preferred of the ones available in CFX. [8][3] This is a hybrid model using the Wilcox  $k-\omega$  model [23] in near-wall regions, and the standard  $k-\epsilon$  model in the fully turbulent region far away from the wall. To ensure a smooth transition between the two models, blending functions are provided in the transitional region for SST-modelling in CFX.

Perrig [2] used this model and showed [24] that the standard  $k-\epsilon$  turbulence model provides unsatisfactory results for the bucket regions, where the flow undergoes high shear stresses, such as the splitter sides and the cutout. [25] demonstrates the superior performance of this model by conducting a large number of validation studies. Further details on the workings of the turbulence model will not be presented in this thesis.

### 2.2.3 Multiphase Modeling

Multiphase flow is characterized as a flow in which more than one fluid is present, e.g. the water jet in the Pelton turbine. Earlier numerical research on Pelton turbines has either utilized the volume of fluid (VOF) method, or the homogeneous model in A. CFX. [3][26][2][27][1][13]

The VOF model in A. Fluent can model two or more immiscible fluids by solving a single set of momentum equations and tracking the volume fraction of each of the fluids throughout the domain. In the homogeneous model, all fluids share common velocity, pressure, and (if applicable) turbulence fields. This model assumes that the solution fields for each phase are identical, except for the volume fractions. The homogeneous multiphase model is recommended for free surface flows in A. CFX.[8][3]

### 2.2.4 Meshing

A CFD analysis is a numerical simulation of the real world, in a virtual and discrete environment. Today, not even a supercomputer has enough power to simulate every single aspect of a complex fluid flow problem. Approximations have to be made. This does not mean that the solution will be inaccurate, sometimes a problem does not have 3D effects or is not dependent on time. The continuous models and equations need to be converted into discrete counterparts. By discretizing in time and spatial dimensions, the differential equations (A.1) through (A.3) are converted into a set of algebraic equations. These equations can be programmed into a code which is solvable by a computer. Basically, a CAD model of the volume occupied by the fluid is divided into discrete cells, which form a mesh with a finite number of cells.

The mesh structure and properties play an essential role in the overall accuracy of the simulation, convergence and CPU time required. An optimal mesh structure is dependent on the type of flow, the geometry of the fluid and the resolution needed. In most cases, the latter is the limiting factor because computational power and simulation time are both highly dependent on the mesh resolution. To construct a high quality mesh requires experience and a good understanding of the numerics of CFD modeling. A. CFX provides documentation and best practice meshing guidelines that will be followed when meshing the fluid domain.

For CFD applications, a structured mesh is in most cases preferable, because it is often more efficient in terms of accuracy, CPU time and memory. However, complex geometries like the Pelton bucket prevent the use of a structured mesh in some regions. Figure 2.6 depicts the cell types used by ANSYS Meshing (A. Meshing) in 3-dimensional meshes. Hexahedral or prismatic elements offer most structure to the mesh, while the tetrahedral and pyramidal elements are used in unstructured areas.

Generally, mesh quality is determined by mesh uniformity, cell size continuity, cell aspect ratio and skewness:

- The cell size  $\Delta x$  should be a continuous function with smooth variation. Cells of very different sizes next to each other should be avoided.
- Aspect ratio is a measure of the stretching of the cell (e.g.  $\Delta x/\Delta y$  for 2D). The smaller the better, but < 100 is considered good in A. CFX. The flow

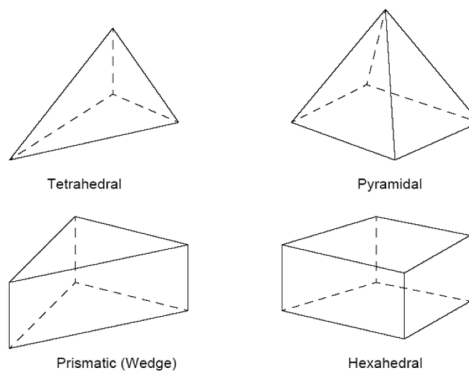


Figure 2.6: Mesh cell/element types in A. Meshing. [7]

should be aligned with the long edge of the element.

- Cell skewness is defined as the cell's angular deviation from its original shape. Concave cells or cells with too small angles between two adjacent edges should be avoided.
- One should pay special attention to grid quality in areas where the flow undergoes rapid variations resulting in big gradients.

A. CFX employs a vertex-centered scheme for which the fluid flow variables are stored at the cell vertex, and the solver-element or control volume is a "dual" of the mesh-element. [7] This means that the vertex of the mesh-element is the center of the solver-element and skewness becomes irrelevant as a quality measure. The CFX solver calculates 3 important measures of mesh quality (Table 2.1) at the start of a run, and updates them each time the mesh is deformed. The expansion factor measures how poorly the nodal position corresponds to the control volume centroid and the orthogonal angle (Fig. 2.8) is defined as  $90^\circ - \text{acos}(\mathbf{n} \cdot \mathbf{s})$ .

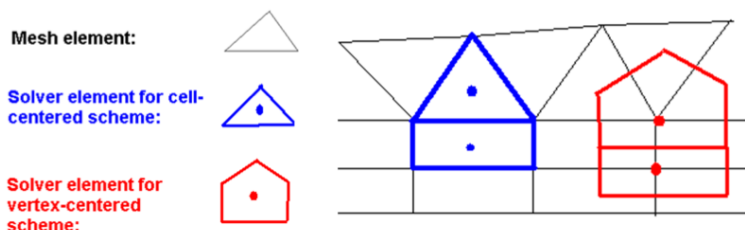


Figure 2.7: Cell-centered vs. vertex-centered. [7]

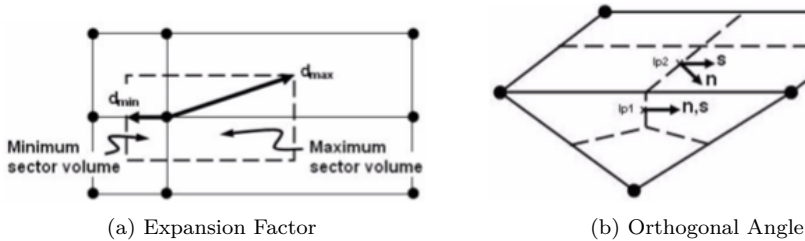


Figure 2.8: Mesh quality for A. CFX. [7]

Table 2.1: Mesh quality thresholds for A. CFX. [8]

Type	Good	Acceptable	Poor
Min. Orthogonal Angle	$> 50$	$50 > 20$	$< 20$
Max. Expansion factor	$< 5.0$	$5.0 < 20.0$	$> 20.0$
Max. Aspect ratio (single precision)	$< 100.0$	$100.0 < 1000.0$	$> 1000.0$

### 2.2.5 Verification & Validation

In the world of computational fluid dynamics, one defines the term verification as:

*The process of determining that a model implementation accurately represents the developer's conceptual description of the model and the solution to the model. [28]*

In other words; the verification should provide evidence that the computational model is solved correctly and accurately. A verification process may involve checking the code, iterative convergence, consistency (e.g. mass conservation), spatial and temporal convergence. One should be able to estimate the accuracy and error of the calculation.

Validation, often interchanged with verification, can be defined as:

*The process of determining the degree to which a model is an accurate representation of the real world from the perspective of the intended uses of the model. [28]*

This implies that the validation of the CFD model should provide evidence that the mathematical model accurately relates to experimental measurements. When a model has been validated, one is able to quantify the model uncertainty. An important aspect of validation, is that it impossible to validate the entire code, only for a specific range of applications for which there is experimental data. The validation process involves the verification described above, comparison of the CFD results with experimental data or DNS, and checking model dependency (e.g. uncertainty in turbulence model). [19]

# Chapter 3

## CFD Analysis

### 3.1 Objective and Challenges

The main objective of this thesis is to establish and validate a CFD model that predicts the *torque* applied to a non-stationary Pelton bucket, subject to a high-speed water jet.

When dealing with non-stationary fluid domains, the numerical analysis itself will be transient, meaning that the flow is unsteady and time-dependent. Data obtained from this analysis can be used to set up a steady-state model of the torque on a Pelton runner. The main challenges regarding this analysis are listed below:

- Large domain (three-dimensional)
- Two-phase, transient simulation
- High speed free surface flow
- Complex mesh/grid (CFD)
- Stationary and rotating domains
- High computational cost (large/dense computational grid)

### 3.2 Methodology

A CFD approach was chosen over SPH, simply because the latter one is in an early development stage. The SPH approach would have resulted in a far more narrow objective.\*

Figure 3.1 is a sketch based on a method DynaVec has experimented with. Basically, the idea behind this method is that the middle bucket is subject to one, complete water-jet cycle. Data obtained from this bucket can be used to model the total runner torque. In Figure 3.1, the *rotating domain* containing the buckets

---

\*Solemslie is investigating the flow in a Pelton bucket using SPH.

is in the initial position. From then on, this domain slides downwards along the *stationary domain*. The simulation stops when the last bucket has cut through the water-jet completely. When modeling the fluid domain, it is important to make sure that the water-jet is fully developed before the first bucket interacts with the water-jet. With this in mind, the initial position of the rotating domain is crucial.

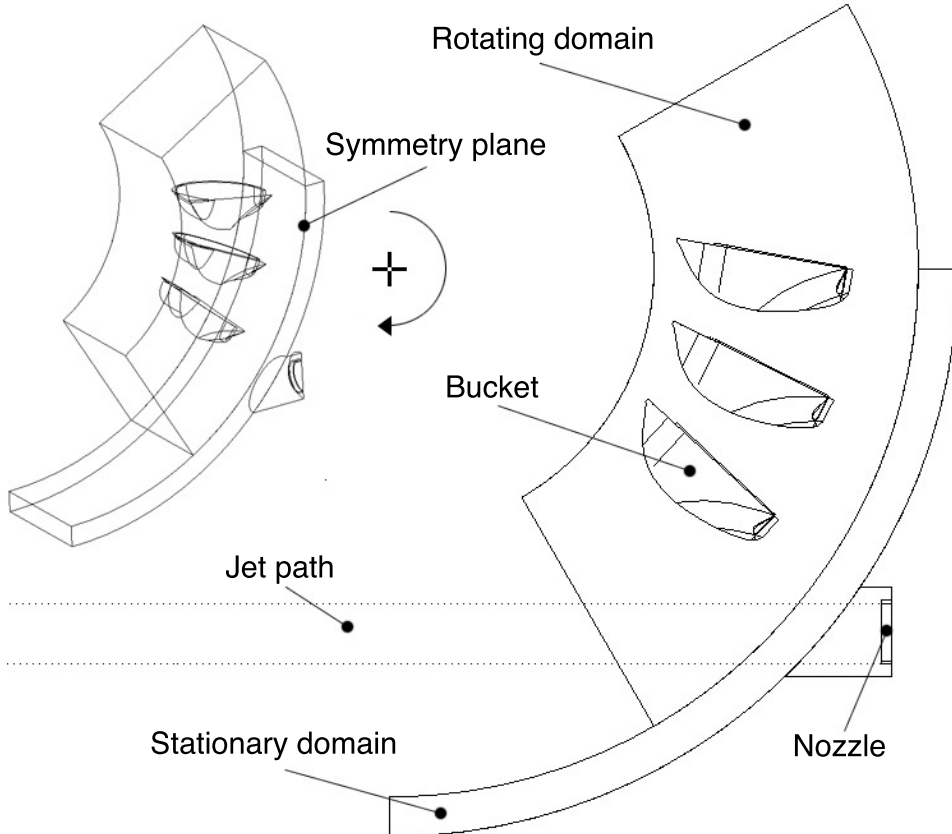


Figure 3.1: Example sketch based on DynaVec's CFD Setup.

To reduce computational cost, the buckets, nozzle and water-jet are cut in half at the symmetry axis. The computational domain is defined by the *rotating domain*, *stationary domain* and *nozzle*. These parts are three-dimensional bodies where the equations in Appendix A are solved for both water and air. The Pelton bucket geometry is placed inside the *rotating domain*, and the volume this geometry occupies is subtracted from the *rotating domain*. The result is a quarter of a disk with three hollow pelton shapes.

The geometric simplifications of this method is the lack of a turbine casing and the simplified nozzle. A turbine casing would cause a back flow of water, affecting the runner and water jet, thus reducing the efficiency. Losses in the nozzle must

be defined using an inlet velocity profile. The air surrounding the buckets also poses as a simplification, because the air is saturated with small water droplets in a steady-state situation. When the buckets start rotating the fluid domain is filled with air of zero velocity, and losses due to air resistance are most likely too small. A steady-state situation will obviously never be reached using this method.

Perrig [2] used the same technique with five buckets instead of three. The advantage with this solution is that three buckets will experience one, complete water-jet cycle. This is favorable because the data obtained from the three middle buckets should be identical and therefore any numerical error in the model will be revealed. As a result, the possibility to create a periodic simulation arises. Imagine that the rotating domain in Figure 3.1 is aligned with the stationary domain. When the rotating domain leaves this position, another identical domain is introduced at the top (the same geometry). Thus, one achieves a continuous simulation of a runner. With this approach it is important that one is aware of the fact that the number of buckets must be correct in comparison with the complete runner. When the water-jet is fully developed one could reach steady state. Obviously, the drawback with this approach is the high computational cost.

In this thesis the three bucket approach will be used because computational cost is a limiting factor at NTNU.

### 3.3 Workflow

A complete workflow for one simulation is presented in this section. This includes CAD modeling of the fluid domain, generation of a computational mesh, physical setup and post-processing. Figure 3.2 depicts the resulting CFD case, ready to run, in ANSYS Workbench.

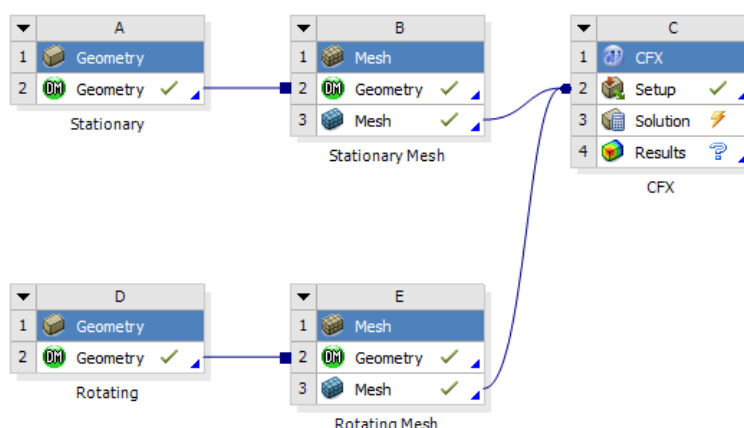


Figure 3.2: ANSYS Workbench overview of a simulation.

### 3.3.1 CAD Modeling with ANSYS DesignModeler

The fluid domain was initially CAD modeled with an application called Pro/Engineer, but ANSYS own CAD modeling application, DesignModeler, proved to be more effective in this particular case. The main reason for this was that the geometries making up the domain are fairly simple. If one were to tweak the bucket geometry between simulations, Pro/Engineer or a similar application would have been the best choice.

Figure 3.3 depicts the completed CAD drawings of the rotating and stationary domain which is modeled separately and assembled here to show their relative initial positions. The green upper part along with the nozzle will be fixed in this position while the brown and grey part will rotate during the simulation. A complete workflow of the CAD modeling is presented in Appendix C.

Originally both domains were 90 degrees, but were later extended 30 degrees. The reason for this was that the torque measurement was incomplete ( $\tau \neq 0$  at the end of the simulation) with a 90 degree domain.

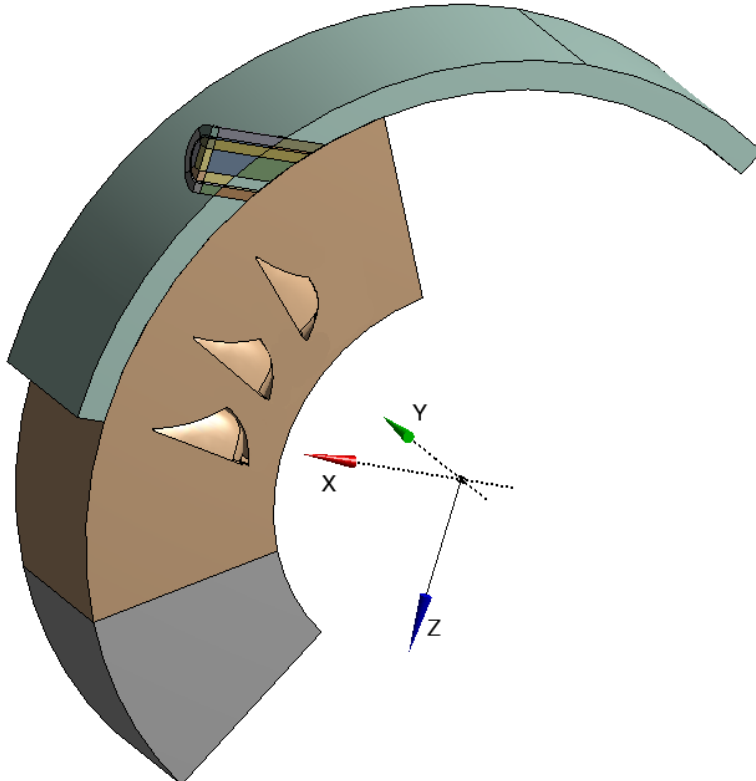


Figure 3.3: Assembly of the rotating and stationary domain.

### 3.3.2 Meshing with ANSYS Meshing

As shown on Figure 3.2, the meshing of the fluid domain was divided in two standalone meshing components, one for the stationary domain and one for the rotating domain. The main reason for this was that the rotating domain was meshed with an advanced size function, while the stationary domain did not use this feature. It is not possible to use this feature on specific parts, it is applied to whole geometry. A complete workflow of the meshing is presented in Appendix E.

The stationary domain was meshed with the advanced size function turned off and consists mostly of hexahedral elements with some prismatic elements around the jet core and jet domain. Sweeping gives a high degree of structure in a mesh, and this method was used on the jet and the surrounding domain. ANSYS Meshing 13.0 actually does a great job meshing the large part automatically. An inflation in the radial direction was applied at both sides of the air-water interface at the jet surface, to better cope with the two-phase interface.

The rotating domain was meshed with the advanced size function "Proximity and Curvature" and consists mainly of tetrahedral elements. To cope with the high velocity water jet in the region of interest, which was the area where the jet interacts with every bucket, the "body of influence" sizing type was used to increase the element density in this area. The same method was used at the outlet of the last bucket to capture the back flow giving a negative torque contribution to the middle bucket.

### 3.3.3 Physical Setup with ANSYS Pre

In this section the essentials of the ANSYS Pre setup are presented. A detailed setup is located in Appendix E. DynaVec did not only provide a bucket geometry, they were also very helpful when it came to the Pre setup. They have experience with similar simulations and shared their findings.

#### Analysis Type

In each "Flow Analysis" in ANSYS Pre there is a tab called "Analysis Type". This is where one defines whether or not the simulation is transient or steady-state, control simulation time and time steps. In this case the transient option with adaptive time steps was chosen.

With adaptive time steps and the option "Num. Coeff. Loops" chosen, the solver automatically adjusts the time step size based on the number of coefficient loops used in solving the current time step. The user can specify the max/min target coefficient loops. If the actual number of coefficient loops used is greater than the maximum target, the time step size is decreased. If the actual number of coefficient loops used is less than the maximum target, the time step size is increased.[8] An

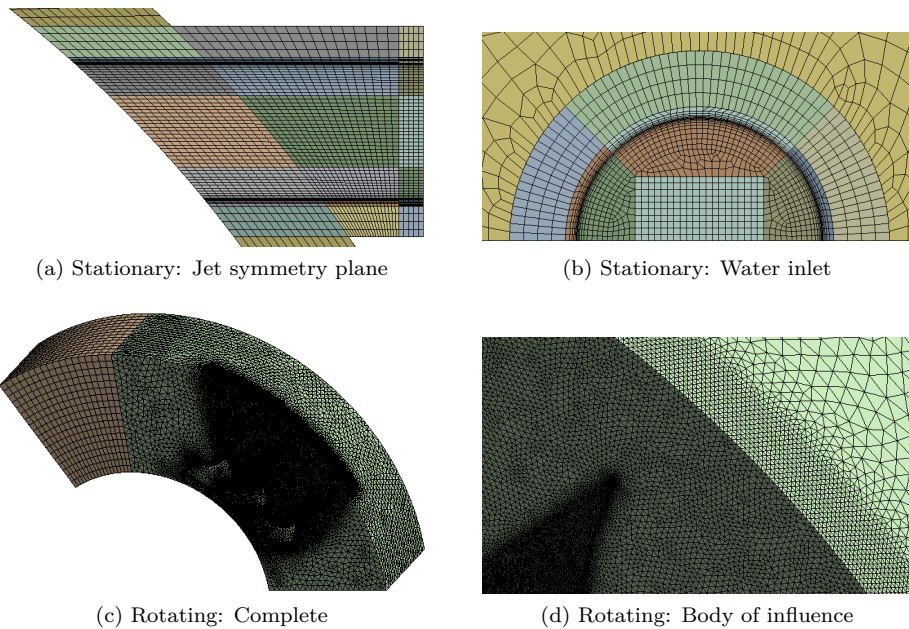


Figure 3.4: Mesh

adaptive time step will ensure that the the resources available are fully exploited because the time step will always be close to the largest possible time step for convergence.

The time duration option was set to "Total Time" with the expression "TotalTime" from Table E.1. This expression equals the time it takes for the rotating domain to rotate 120 degrees.

## Domains

Two fluid domains were created, one for the rotating part and one for the stationary part. As stated in Section 2.1.1, there is no pressure difference between the inlet and outlet of the runner. In most cases the pressure is atmospheric around the turbine and therefore the reference pressure in both domains were set to  $1atm$ . In the Pelton rig in the laboratory a small underpressure can arise if the turbine housing is fully sealed. This difference was ignored.

In free surface flows the homogeneous multiphase model should be used when possible. [8] The flow in a Pelton turbine is under gravity and the interphase flow could be considered to be drag dominated because the air velocity relative to the jet is very low. These properties qualifies the flow for the use of the homogeneous model. However, the model does not apply to droplets falling under gravity in a gas. Water droplets will obviously occur in a Pelton turbine, but the flow of interest does not

depend of these droplets. At the same time these droplets will probably have a high velocity relative to the surrounding air making the gravity force contribution small in comparison. Based on the above, the flow in a Pelton turbine fulfills the requirements of the homogeneous model reasonably well, therefore this model was chosen for both domains.

The standard free surface model was chosen because the air-water interface can be considered distinct. [8] The surface tension coefficient was set manually to  $\sigma = 0.0728 \text{ Nm}^{-1}$  [6], and the surface tension model Continuum Surface Force with the primary fluid as water was also chosen. This model is based on the Continuum Surface Force model of Brackbill et al. [29].

As presented earlier, the SST turbulence model was found to be the best choice.

Heat transfer is neglected in this case although there is a small temperature difference before and after the energy conversion in the runner. Friction in the bucket converts kinetic energy into heat, thus a temperature difference will occur.

For initial conditions, the cartesian velocity components were set equal to zero and the volume fraction of air and water were set to 1 and 0 respectively. An initial velocity field equal to zero is a simplification and does not produce the desired steady-state behavior of the flow when the torque of the middle bucket is recorded. This is an inevitable drawback with the three bucket approach.

The interface model General Connection and the frame change/mixing model Transient Rotor Stator were chosen. The General Connection model allows the connection of non-matching grids and fully transient sliding interfaces between domains. The Transient Rotor Stator frame change/mixing model predicts the true transient interaction of the flow between a stator and rotor passage at a high computational cost. In this case the grid of the rotating domain and stationary domain do not match, and transient effects across the interface must be captured. With pitch change, dissimilar meshes can be connected, and an intersection algorithm is used to find the overlapping parts of the mesh face at the interface. In this case both interfaces are similar and the simulation is non-periodic, thus the pitch ratio was set manually to 1.

To apply a rotation to the rotating domain, Domain Motion in the rotating domain was set to Rotating, and Angular Velocity was defined by the expression "Omega". In this case the angular velocity is positive because the domain was modeled to rotate in the positive rotation direction about the y-axis. The unknown friction losses in the nozzle was not accounted for in the calculation of "Omega" i.e.  $\varphi = 1$  in Equation (2.4).

### Boundary Conditions

In Figure C.12 and C.9 the boundaries are depicted. The top (T) , middle (M) and bottom (B) bucket have two boundaries each. "MB" refers to the main flow

region inside the middle bucket and "MBC" refers to the total surface of the middle bucket.

The buckets were defined as no slip, smooth walls.

The boundary "RotOpen" (Figure C.12) was defined as an opening with an air volume fraction of 1, which allows air to simultaneously flow in and out of the domain. When water flows into the rotating domain, air will be pushed out of the openings and the atmospheric pressure is maintained.

The boundaries "RotSym" and "StatSym" were defined as symmetry which makes this plane geometrically and flow symmetric.

The boundary "JetWall" was defined as a wall, which according to DynaVec, gives a better jet stability. A drawback with this solution is that the drag force created by the jet close to the nozzle is presumed to suck air from the surroundings, thus this effect is reduced.

The boundary "JetInlet" was defined as an inlet with the normal inlet speed equal to the expression "InletVel". This is obviously a great simplification due to the lack of a needle and uniform velocity profile. However, the aim of this thesis is to establish a working CFD model and optimization was considered as future work. Using the expression "InletVel" and "Omega", results in an optimal theoretical operating condition.

DynaVec recommended that the boundary "StatInlet" should be defined as an inlet with a small air velocity. They have experienced a better stability with this method. Naturally this was the obvious starting point.

## Solver Control and Output

The default transient scheme, Second Order Backward Euler, was chosen because it is recommended by ANSYS [8] for most transient runs. The minimum number for coefficient loops was set to 3 to ensure that at least 3 iterations are completed per time step. According to [8], 10 coefficient loops per time step is usually adequate to resolve the strong non-linearities in multiphase flows, thus the maximum number of coefficient loops was set to 10. If convergence is not sufficient with this number of coefficient loops, one should reduce the time step size rather than increase the number of coefficient loops.

The residual is the most important measure of convergence, as it relates directly to whether or not the equations have been solved. A residual level of  $10^{-4}$  is considered as a relatively loose convergence by ANSYS, but may be sufficient for many engineering applications. Values above this level may be sufficient to obtain a qualitative understanding of the flow field. In this case, the residual type RMS (root mean square) was chosen with a residual target of  $1.15 \times 10^{-4}$ . With a target that is 1.15 times higher than the recommended value for loose convergence, the results are considered to be sufficient enough to obtain a qualitative understanding of the

flow in a rotating Pelton bucket. A target of  $10^{-5}$  is ideal for good convergence, but in this case this was not possible due to the limiting computational resources.

The main output of the simulation is the total torque on the middle bucket. A monitor for the expression "TorqueMBC" was added, which logged the torque and made it possible to monitor the torque during the simulation. Initially, complete transient results were logged 10 times at a fixed time step. After studying the torque curve from the initial run, specific points of interest in time, were chosen manually as the output points.

### 3.3.4 Post-Processing

This section describes the method used for creating the total torque curve, based on a single numerical bucket measurement. In principle, this problem is quite simple, but varying time step size due to the adaptive timesteps and point specific bucket frequency  $f_Z = \frac{\omega \cdot Z}{2\pi}$  complicated this task.

To calculate the complete torque on the runner, the torque from a single bucket was duplicated  $n$  times and each duplicate was shifted  $n \cdot \frac{1}{f_Z}$  in time. This imitates  $n$  buckets passing the jet. In Figure 3.5 the principle is visualized. In this case a steady-state reading of the total torque could be extracted from  $t = 5 \cdot \frac{1}{f_Z}$  to  $t = 9 \cdot \frac{1}{f_Z}$ .

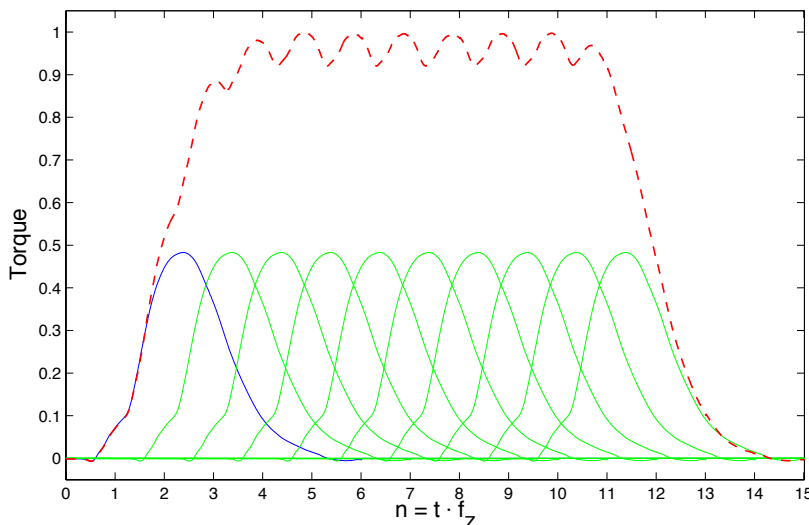


Figure 3.5: Total torque on runner (red) calculated from duplications (green) of a single numerical torque measurement (blue).

The torque data from the analysis was processed in MATLAB. The varying time

step size lead to some difficulties because the torque measurements for two buckets would not match up when one bucket is shifted  $\frac{1}{f_Z}$  [s] in time. To solve this problem a fixed time step size was calculated so that two time series align when one is shifted  $\frac{1}{f_Z}$  [s]. The MATLAB script for the post-processing is found in Appendix F.

## 3.4 Simulations

The CFD model has undergone mesh dependency tests and been tested at different heads. An overview of the setup used in all simulations is presented in Table 3.1. In Chapter 4, the results of these tests are compared with experiments conducted in the laboratory.

Table 3.1: Overview of the basic setup used for all simulations.

<b>Solver</b>	ANSYS CFX 13.0
<b>Time discretisation</b>	Transient
<b>Advection scheme</b>	High Resolution
<b>Transient scheme</b>	Second Order Backward Euler
<b>Turbulence model</b>	SST with automatic wall function
<b>Multiphase model</b>	Homogeneous model + Std. Free Surf. Model
<b>Surface tension model</b>	Continuum Surface Force (primary fluid → water)
<b>Surface tension coeff.</b>	$\sigma_1 = 0.7$ and $\sigma_2 = 0.0728$ , [N/m]
<b>Convergence criteria</b>	RMS, Residual target = $1.15 \times 10^{-4}$
<b>Hardware</b>	Processor: Intel Xeon X5650 2.67 and 2.66 GHz ( $2 \times 6 = 12$ cores). Memory: 24 GB

### 3.4.1 Surface Tension Coefficient

After all simulations were conducted, a possible error was discovered in the ANSYS Pre setup. The water surface tension coefficient was set to  $\sigma_1 = 0.7$  N/m, which really should be 0.0728 N/m according to White [6]. DynaVec had used 0.7 N/m, and their source was EDR Support [30]. After discussing this matter with DynaVec and EDR support, it was concluded that the surface tension coefficient from White should be used.

All simulations in Table 3.2 and 3.4 were ran a second time with a surface tension coefficient  $\sigma_2$ . Despite the extra time spent on simulations, the opportunity to investigate the effect of decreasing the water surface tension by a factor of  $\sim 10$  arose. Klemetsen [3] concluded that the surface tension among other properties like gravity, viscosity and turbulence could be neglected. This observation is possible to test.

### 3.4.2 Mesh Dependency

The purpose of a mesh dependency study is to find a mesh size  $M_I$ , where a parameter  $y$  of interest will remain constant if  $M$  is increased. Then  $M_I$  would be the best choice because a finer mesh would not affect the solution. One generally favors a mesh independent solution, but mesh independence is not a requirement for achieving good results. The parameter  $y$  could easily converge far away from the real solution  $S$ , and pass  $S$  in the process. In this case a courser mesh ( $< M_I$ ) could produce a more physical correct result.

In accordance with the main objective of this thesis, it was of interest to find the mesh size where the total torque  $\tau$  is constant if the mesh size is increased any further. Because the torque is proportional to the efficiency of the turbine ( $\eta_h = G(\omega, \rho, Q, H, g) \times \tau$ ), it is important to achieve mesh independence in order to estimate the error of the CFD results. An overview of the mesh dependency simulations are presented in Table 3.2.

Eight different mesh sizes were tested with an effective head of  $75m$ . The mesh size on the rotating domain is controlled by two main variables; the middle buckets inner surface element size (FS) and the body of influence (BoI) element size. The mesh size on the stationary domain is mainly controlled by the inflation on the jet's air-water interphase. These areas were considered to be most important for this particular case. The first layer height (FLH) of the inflation inside the middle bucket was held constant at approximately  $0.1mm$ .

### 3.4.3 Head

The purpose of these tests was to investigate if the deviation between the CFD model and the experiments was constant for varying heads. If the deviation is constant, the head aspect of the model validation process can be excluded as a source of error.

Four simulations using the mesh from the mesh dependency test MD3, were ran at varying heads (Table 3.4). This mesh was chosen because of its relative low size and successful simulation on  $75m$ .

Table 3.2: Overview of the mesh dependency tests. These simulations were done two times, to compare two surface tension coefficients ( $\sigma_1$  and  $\sigma_2$ ). 16 simulations in total at  $H_e = 75[m]$ .

Name	SE $\times 10^{-5}$	RE $\times 10^{-5}$	TE $\times 10^{-5}$	FS [mm]	BoI [mm]	FLH [mm]
MD1	0.2	17.1	17.3	2.0	4.0	0.1
MD2	1.6	23.2	24.8	1.0	2.2	0.1
MD3	1.6	27.7	29.4	0.8	2.1	0.1
MD4	1.6	33.6	35.2	0.7	1.8	0.1
MD5	2.4	43.2	45.6	0.6	1.6	0.1
MD6	2.4	55.0	57.3	0.5	1.35	0.1
MD7	1.6	68.4	70.1	0.5	1.2	0.08
MD8	2.4	68.4	70.8	0.5	1.2	0.08

**SE:** Number of elements in the stationary domain  
**RE:** Number of elements in the rotating domain  
**TE:** Total number of elements  
**FS:** The middle buckets inner surface element size  
**BoI:** Body of influence element size  
**FLH:** First layer height of the inflation inside the middle bucket

Table 3.3: Mesh characteristics showing the amount of nodes [%] that fulfills the "Good" quality requirement in Table 2.1.

Mesh	Orthog. Angle		Exp. Factor		Aspect Ratio	
	Stat.	Rot.	Stat.	Rot.	Stat.	Rot.
MD1	98	100	100	97	100	100
MD2	98	100	100	98	100	100
MD3	98	100	100	98	100	100
MD4	98	100	100	98	100	100
MD5	99	100	100	98	100	100
MD6	99	100	100	98	100	100
MD7	98	100	100	99	100	100
MD8	99	100	100	99	100	100

Table 3.4: Overview of the Head tests. These simulations were ran two times (8 simulations), to compare two surface tension coefficients ( $\sigma_1$  and  $\sigma_2$ ).

Name	Head [m]	Mesh
H1	40	MD3
H2	60	MD3
H3	70	MD3
H4	80	MD3

## 3.5 Results

All simulations for both  $\sigma_1$  and  $\sigma_2$  finished successfully, except for MD1. Table 3.5 presents the convergence status, RMS courant number and simulation time for the  $\sigma_2$  simulations. Convergence was generally good and behaved consistently more or less like the MD8 ( $\sigma_2$ ) simulation in Figure 3.6.

Table 3.5: Overview of the simulation results. Surface tension coeff. =  $\sigma_2$ .

Name	Convergence	RMS Courant	Sim. time
		$\approx$	[h]
MD1	Failed	-	-
MD2	OK	0.4 – 2	19
MD3	OK	0.7 – 2.2	21
MD4	OK	0.9 – 3	24
MD5	OK	0.6 – 2	37
MD6	OK	0.8 – 2	36
MD7	OK	0.5 – 2	39
MD8	OK	0.9 – 1.6	44
H1	OK	0.5 – 2.4	27
H2	OK	0.6 – 2.6	23
H3	OK	0.5 – 2.2	23
H4	OK	0.7 – 2.4	20

**Convergence:** Solution convergence target fulfilled

**RMS Courant:** RMS Courant number

**Sim. time:** Total simulation time (wall clock)

Every successful simulation produced a torque measurement as depicted in Figure 3.7. Overall, the repeatability of the torque signature is good in terms of phase and general characteristics. The same could be said for the head simulations depicted in Figure 3.8.

Figure 3.9 depicts the mesh dependency results. At approximately  $4.5 \times 10^6$  elements the solution seems to become independent of the mesh size.  $\sigma_2$  has a more stable development than  $\sigma_1$  in this region. MD8 ( $\sigma_1$ ) drops considerably relative

to the other simulations of this mesh size.

A visualization of the flow through the middle bucket duty cycle is depicted in Figure 3.11. From a visual perspective, the flow behaves as expected (discussed in Section 3.6.3).

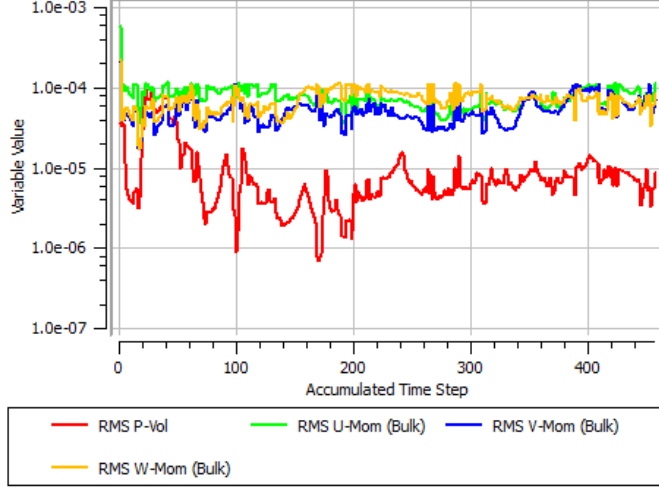


Figure 3.6: Mass and momentum residuals for MD8 ( $\sigma_2$ ).

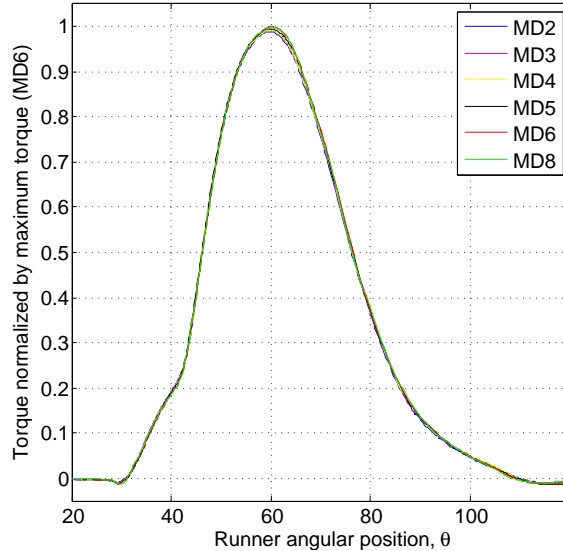


Figure 3.7: Middle bucket torque for simulations with the surface tension coeff.  $\sigma_2 = 0.0728[Nm^{-1}]$ .

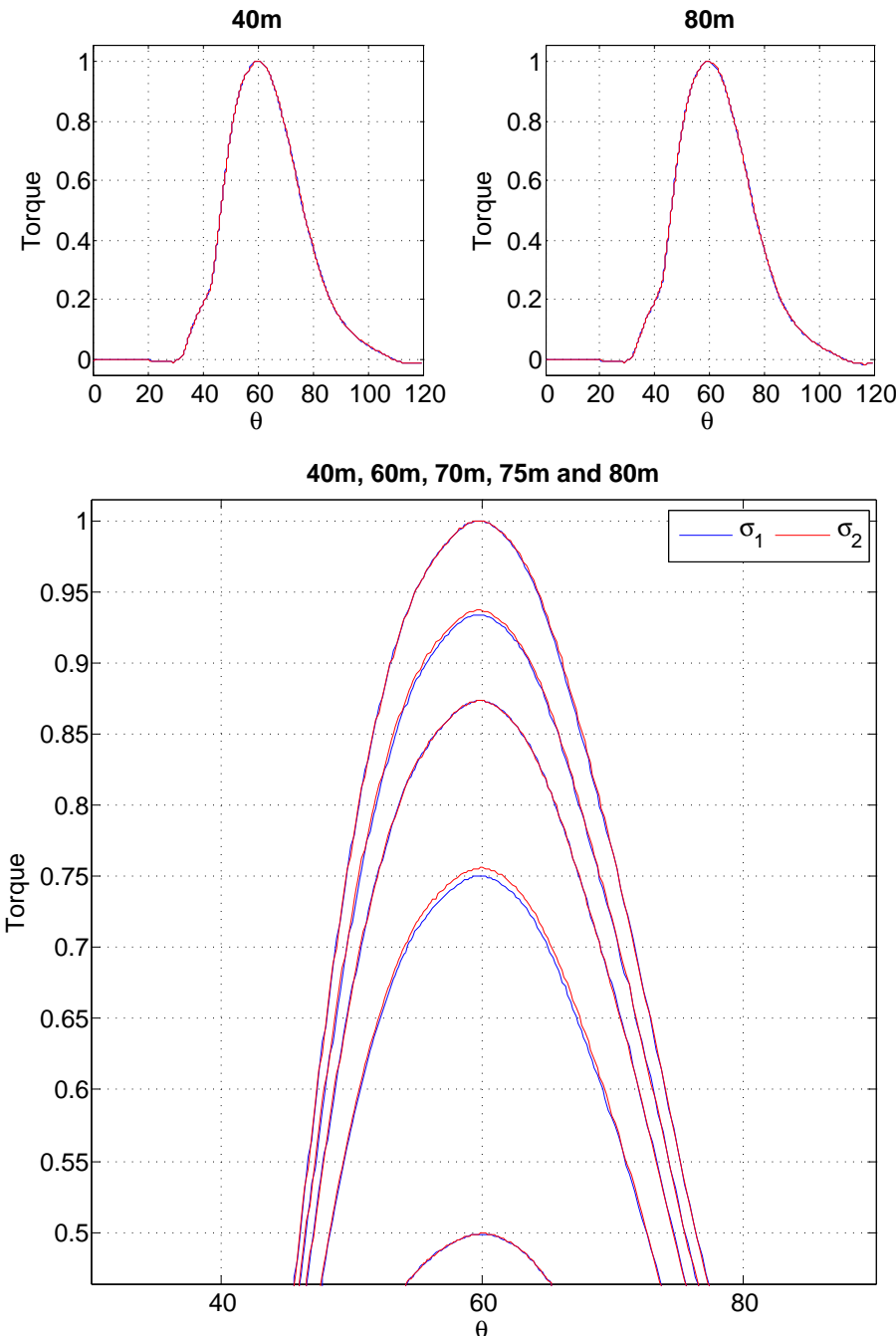


Figure 3.8: Comparison of the middle bucket torque with different surface tension coefficients;  $\sigma_1$  (blue) and  $\sigma_2$  (red). The torque is normalized with  $\tau_{\sigma_2}$  and the tests use the MD3 mesh.

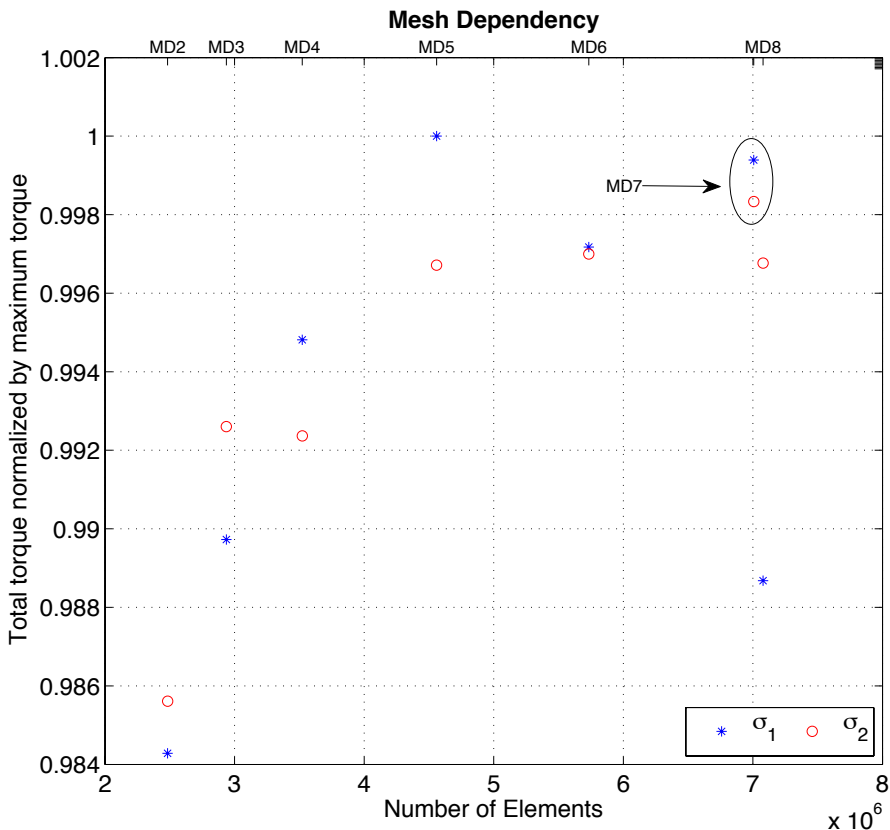


Figure 3.9: Mesh dependency results.

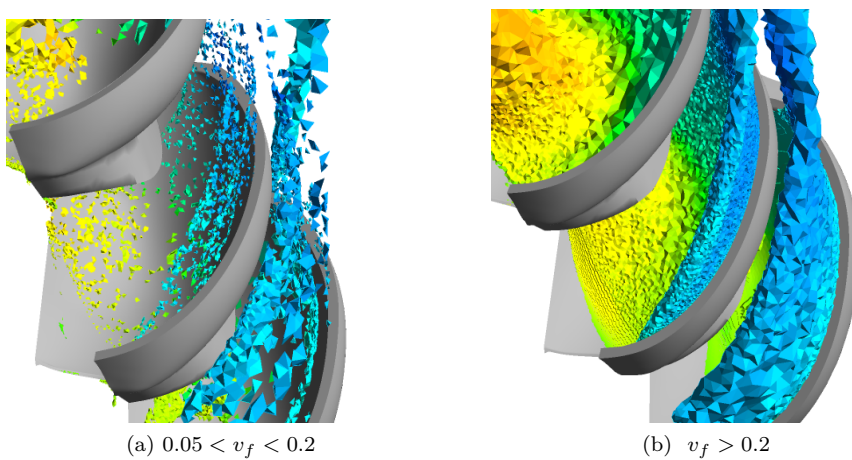


Figure 3.10: Volume fractions in frame 9 (Figure 3.11).

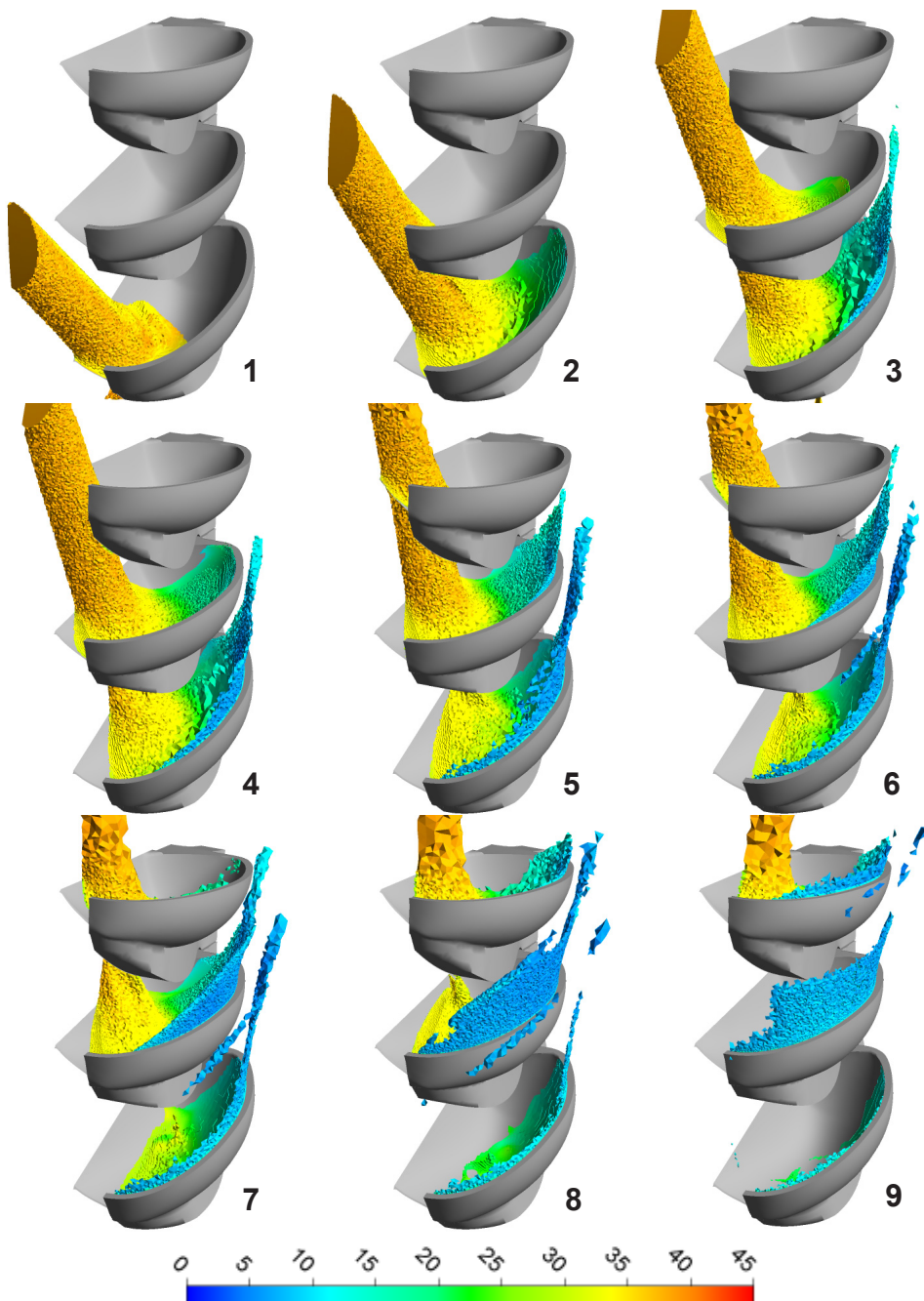


Figure 3.11: Flow visualization for the MD8 simulation. All cells with a water volume fraction above 0.7 are displayed, and the color range represents the velocity [ $m/s$ ]. Angular position: (1)  $27^\circ$  (2)  $37^\circ$  (3)  $48^\circ$  (4)  $56^\circ$  (5)  $60^\circ$  (6)  $64^\circ$  (7)  $70^\circ$  (8)  $77^\circ$  (9)  $88^\circ$

## 3.6 Discussion and Verification

All simulations successfully produced a torque measurement on the middle bucket, except the MD1 simulations. The main difference between MD1 and the rest, is that MD1 has almost twice the element size in the bodies of influence (Section 3.3.2) than MD2. At the same time the stationary domain has a very coarse mesh compared to the other simulations, which probably was the cause of the failure. Inspections of the flow in the stationary domain showed that the jet failed to develop properly. Furthermore, when entering the rotating domain, the flow also failed to maintain its straight profile and bended towards the negative rotational direction. As a result of this, the torque measurement on the middle bucket failed completely.

From MD2 to MD8, the simulations produced good results in terms of capturing the basic flow characteristics of what would be expected of the flow in a Pelton bucket. An example of this is shown in Figure 3.11 and discussed later in this section. Figure 3.7 displays the torque measurements on the middle bucket, which could be considered fairly consistent throughout the mesh size range. The torque curves have a high repeatability when it comes to the general torque signature, and the main difference between them is found in the peak torque readings. At varying heads these characteristics are still valid as seen in Figure 3.8. Based on the results, a mesh size equal to MD2 is the absolute minimum for achieving a successful run.

The objective of the MD7 simulations was to test the importance of a high element count in the stationary domain. MD7 was conducted with the same rotating mesh as MD8 and a low mesh size on the stationary domain (same as MD2-4). MD7 is not considered in the mesh dependency evaluation because it only changes in the stationary domain. In retrospect, it probably would have been best to use a constant mesh size for the stationary domain. In that way a comparison of the rotating mesh, where the torque measurement takes place, would probably offer a better consistency.

Figure 3.8 depicts the results of the head tests, where the blue and red curves represent the surface tension coefficient  $\sigma_1$  and  $\sigma_2$ , respectively. Like MD2-8, H1-4 successfully produced a torque measurement for one bucket duty cycle. The torque signature is also maintained throughout the head range. This proves that the model has a good numerical repeatability for the tested head range.

Overall, the mesh quality is good, as shown in Table 3.3. Hence, the numerical errors stemming from the mesh are in this case considered to be minor. Some elements ( $< 1\%$ ) could be categorized as poor according to [8]. However, the amount and location of these elements suggests that they will not affect the solution.

In this case  $y^+$  is difficult to analyze because the contact fluid at the wall (buckets) continuously changes between air and water as the buckets rotate. Therefore,  $y^+$  was not evaluated, but a solution to the measuring of  $y^+$  would be a good supplement to this thesis.

### 3.6.1 Mesh Dependency

In Figure 3.9 the total torque for the mesh dependency tests are plotted against mesh element size. At  $4.5 \times 10^6$  elements the solutions can be considered mesh independent for both  $\sigma_1$  and  $\sigma_2$ . However,  $\sigma_2$  has a smaller deviation in this region, which favors  $\sigma_2$  as a slightly better representation of the surface tension coefficient in terms of repeatability.

The author has no explanation as to why the MD8 ( $\sigma_1$ ) simulation produced a low torque measurement compared to rest of the simulations above MD5. Both simulations completed normally and converged within the target.

The MD7 simulation showed that the mesh size on the stationary domain, in fact has an impact on the solution. The torque increased for both  $\sigma_1$  and  $\sigma_2$ , but the increase for  $\sigma_1$  was more significant than for  $\sigma_2$ .  $\sigma_1$  is actually higher than  $\sigma_2$  in MD7, which is the opposite of MD8. It is difficult to explain this behavior, but based on the other results it seems that  $\sigma_1$  results in a more elastic solution. In other words, the solution may be more sensitive to a higher  $\sigma$ . After discussing the surface tension coefficient with EDR Support [30], their answer to this matter was that one often vary  $\sigma$  from case to case, even if the fluid pair (e.g. air-water) is the same. This implies that one choose a  $\sigma$  that stabilize the solution and accurately represents the conceptual model. The difference between the tested surface tension coefficients is not large, but if one were to choose,  $\sigma_2$  will probably offer a more stable solution.

Given that mesh independency occurs at  $4.5 \times 10^6$  elements, the MD5 mesh would be better suited for the head tests. But limiting computer resources prevented this in terms of simulation time (24 vs. 37 hours).

### 3.6.2 Convergence and Stability

MD1, MD2 ( $\sigma_2$ ) and MD6 ( $\sigma_2$ ) had convergence problems. The torque measurement was not affected by this on the MD6 and simulation, but a few iterations at the end of the simulation failed to meet the residual target of  $1.15 \times 10^{-4}$  (RMS). One explanation as to why the torque is not affected by this, may be that when this happens at the end of the simulation the water jet has developed correctly and the flow has obtained the correct flow condition in the bucket. At the same time the flow has entered the high resolution part of the domain, which is the middle bucket and the surrounding bodies of influence. When convergence problems occur early in the simulation, during the first time steps, the jet development can fail and the implications are more severe. This was the case with MD1, where the jet did not develop properly, resulting in total failure for the torque measurement.

The 20 remaining simulations (including the head simulations), successfully converged within the target. Figure 3.6 depicts the momentum and mass residuals for the MD8 simulation.

According to [8], a convergence target of  $10^{-5}$  is usually sufficient for most engineering applications. The target used in these simulations is considered relatively loose, and may only be sufficient to obtain a qualitative understanding of the flow field. Therefore a target of  $10^{-5}$  is recommended, should this model be used in dimensioning turbines and bucket design. Obviously, simulation time and computer resources may increase as it is likely that the time step has to be reduced.

Total simulation time ranged from 19 to 44 hours. For the hardware used in this thesis, one can expect 37 hours of simulation time for a mesh independent solution. There was no substantial difference between  $\sigma_1$  and  $\sigma_2$  in regards of simulation time.

Total time steps varied as the adaptive time step method was used. All simulations had the same minimum and maximum time step limits, including the head simulations. This was probably inefficient because at 40m, 60m and 70m the flow has a lower velocity. When the velocity is increased, a smaller time step is required to capture all transient effects. Thus, to use the same limits at 40m and 80m is probably not necessary. Another inefficient setting used, affecting simulation time and convergence, was the min/max target coefficient loops for adaptive time steps. Minimum and maximum coefficient loops within one timestep were set to 3 and 10, respectively. The adaptive maximum target was set to 8, meaning that the solver either decrease or increase depending on the actual number of coefficient loops used. A target of 4-5 would probably have been better because it would lead to an increased adaption rate.

A. CFX is an implicit solver, thus a low courant number is not required. Still, the average bulk courant number for air and water is low for all simulations.

### 3.6.3 Flow Visualization

A complete visual analysis was not conducted in this thesis because the experimental work was limited to torque measurements only. The following is based on visual studies of the CFD simulations.

In Figure 3.11, nine frames at varying angular positions, visualize the flow through the middle bucket (MB). All cells with a water volume fraction above 0.7 are displayed in a color range representing the water velocity in the cell. The volume fraction was chosen because lower volume fractions cloud up the images. From frame 6 to 9 there appears to be a breakup of the flow and water seems to disappear, but in reality the water volume fraction in these cells are below 0.7.

In frame one the fully developed water jet is approaching the MB cutout. The mesh was designed so that the jet would maintain a high element resolution during the MB cycle, and frame 1-5 show that this has been successful. Also, the body of influence at the outlet of the MB gives a high element resolution at the outlet. As a result of this, a high resolution is obtained from the inlet to the outlet, which reduce big gradients in this crucial area. From frame 6 to 9 the jet enters an area

of coarser elements, but this does not affect the results because at this point the jet does not interact with MB.

The flow velocity behave as expected. The velocity in the incoming jet remains constant throughout all frames and approaches zero some distance from the outlet. By studying frame 6, the gradual energy exchange between the jet and the MB is clearly visible. A small velocity at the bucket outlet is the result of the bucket design and is indeed expected. The theoretic zero outlet velocity would cause accumulation and back splash, thus ruining the efficiency.

Overall it looks like the water coming out the bucket outlets does not touch the bucket above, but Figure 3.11 does not display  $v_f < 0.7$ . In Figure 3.10, cells in frame 7 with  $0.05 < v_f < 0.2$  and  $v_f > 0.2$  are displayed. Still, it looks like the mean water flow indeed clear the buckets (Fig. 3.10b).

By studying the water outlet direction, one observe that the main outlet flow gradually shifts from the back part of the bucket (root) to the front part towards the cutout. This is expected as the jet inlet angle shifts accordingly to the mean flow outlet direction in each frame.

To summarize, the model seems promising from a visual perspective:

- The model predicts the expected flow fairly good, without having verified it against experimental results.
- The energy exchange behave as expected.
- The water jet is fully developed before interacting with the buckets. (Not shown here)
- The bucket outlet flow behave as expected.



# Chapter 4

## Validation of the CFD Model

In this chapter the numerical torque measurements are compared with experimental measurements, with the goal being a validation of the CFD model. The intended use for the model is to predict the runner torque, which again relates to the efficiency, as accurately as possible. A complete validation is not possible due to the fact that other parameters would have to be taken into account. Thus, the validation in this thesis only concerns the torque. The current use of the model should be restricted to torque measurements and nothing else. Naturally, the verification of the simulations in the previous chapter is a part of the validation.

### 4.1 Experiments

The objective of the experimental work was to obtain measurements of the operational points used in the CFD simulations. The measurements were done on a model runner by DynaVec, which is geometrically identical (1:1) with the CAD model used in the simulations.

Suman Aryal, Bidhan Rajkarnikar and Sudip Adhikari performed the laboratory work and supplied the author with raw data.\*

#### 4.1.1 Instrumentation

The Pelton rig in the Waterpower laboratory, depicted in Figure 4.1, was used for the experiments. In January 2012, Kyrre Reinertsen completed a modification to the rig, which introduced the possibility to measure the torque lost to friction in the bearings. [9]

---

\*Aryal, Rajkarnikar and Adhikari are exchange students from Nepal. They stayed at the Waterpower laboratory at NTNU in the spring of 2012, acquiring enough experience to set up a similar Pelton rig at Kathmandu University.

The rig consists of a generator/motor, horizontal axle, adjustable nozzle, pump and watertight turbine casing. Various instruments measure the volume flow, pressure, rotational speed, temperature, generator torque and friction torque. The total torque is equal to the sum of the generator torque and the friction torque.

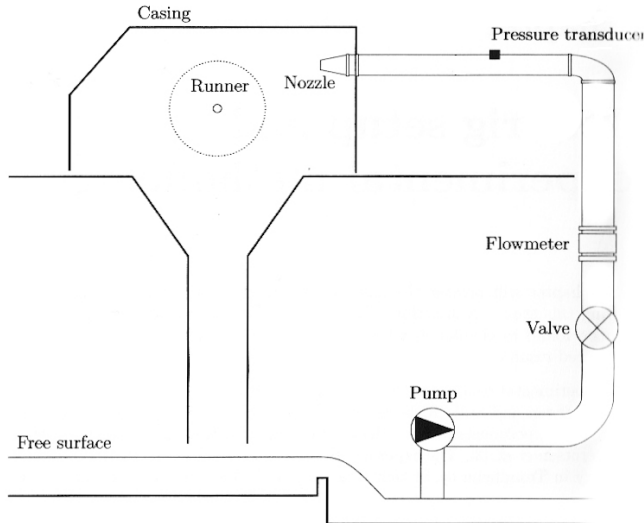


Figure 4.1: NTNU Pelton model rig. [1]

To regulate the flow and reach a desired operational point, three main parameters are regulated from a control room: (1) pump rotational speed, (2) runner rotational speed and (3) nozzle opening.

### Instrument Calibration

Aryal, Rajkarnikar and Adhikari calibrated the torque prior to the experiments, but this calibration was found to be invalid. In order to estimate the uncertainty of the torque measurements, the latest calibrations were used, which were performed by Reinertsen in January<sup>†</sup>. Details regarding the calibration procedures can be found in Reinertsen's MSc thesis [9].

#### 4.1.2 Test Procedure

In Table 4.1 an overview of the experiments is presented. Five individual torque measurements were taken at different operational points corresponding to the CFD simulations. Each operational point was measured two times, on increasing and

---

<sup>†</sup>10.01.2012

decreasing load, respectively. Afterwards, the two measurements were merged together. The recording time for every operational point was 60 seconds with a sample rate of  $\sim 1000s^{-1}$ .

Table 4.1: Overview of the experiments.  $Q$  and  $n$  is normalized with the  $80m$  values.

Experiment	$H_e$ [m]	$Q$	$n$
E1	40	0.707	0.707
E2	60	0.866	0.866
E3	70	0.935	0.935
E4	75	0.968	0.968
E5	80	1	1

Head  $H$  [m], volume flow  $Q$  [ $m^3/s$ ] and rotational speed  $n$  [rpm] were extracted from each simulation and represented the operational points measured experimentally. The volume flow calculation was based on the CAD geometry and jet velocity at the nozzle inlet in the CFD model:

$$Q = c_1 \frac{\pi}{4} d_s^2 \quad (4.1)$$

where  $c_1 = (2gH)^{1/2}$  and  $d_s$  is the diameter of the water jet (inner nozzle diameter) in the CAD model. The rotational speed (4.2) was calculated using the same principle as in the CFD model: *The optimal theoretical efficiency is achieved if the peripheral velocity of the runner is equal to half of the water jet velocity. [31]*

$$n = \frac{30}{\pi} \omega = \frac{30}{\pi} \frac{\frac{1}{2} c_1}{r} \quad (4.2)$$

As stated in Section 3.3.3, the theoretical operational condition was used in the simulations. Using the same operational parameters in the experiments is not optimal. The reason for this is that losses in the nozzle are not accounted, resulting in a too high angular runner velocity. Thus, a lower efficiency is expected in the experimental results.

### 4.1.3 Uncertainty

Reinertsen's calibration data<sup>‡</sup> for the torque and friction torque was used in the calculation of the total uncertainty for each experiment. The method used in the uncertainty calculations is presented in Appendix B.

---

<sup>‡</sup>Available in Reinertsen's MSc thesis [9]

## 4.2 Results

Experimental results are presented relative to the numerical results in Chapter 3. The uncertainty of the experimental torque measurements is presented in Table 4.2. At the turbine's best operational point,  $H_e = 75m$ , the total uncertainty for the torque measurement is 0.1863%.

Table 4.2: Torque uncertainties at varying heads.

Systematic	Constant [%]	Total [%]				
	-	40m	60m	70m	75m	80m
Shaft torque, $f\tau_{gen}$	0.0869	0.2892	0.2007	0.1893	0.1877	0.1880
Friction torque, $f\tau_{fr}$	0.2600	1.3474	1.2168	1.4089	1.2350	1.2779
Total torque, $f\tau_{tot}$	-	0.2854	0.1989	0.1880	0.1863	0.1868

Figure 4.2 depicts the deviation [%] between the experiment  $E4$  and mesh dependency simulations, where  $y = 0$  represents the mean torque measurement of  $E4$  ( $H_e = 75m$ ). For a the mesh independent solution the deviation is approximately 1.5% ( $\sigma_2$ ). Note that the variation between the mesh independent solutions is approximately the same as the uncertainty of the experiment.

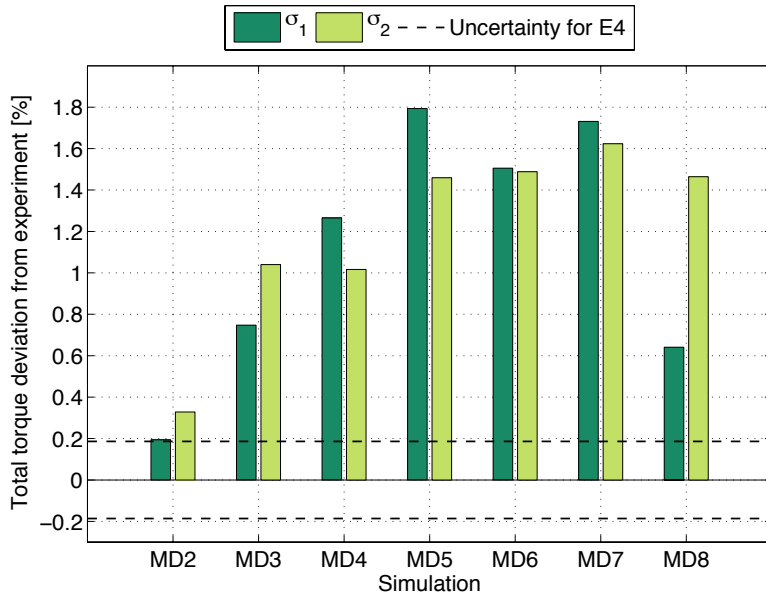


Figure 4.2: Total torque  $\tau_{tot}$  deviation between mesh dependency simulations and corresponding experiment E4.

The deviation between the head simulations and corresponding experiments (H1-

H4) is depicted in Figure 4.3. Here,  $y = 0$  represents the mean torque measurement for each experiment. Because these simulations use the same mesh size as MD3, variation in the deviation between various heads is comparable. The deviation vary between 0.68 – 0.89 % and 0.65 – 1.53 % for  $\sigma_1$  and  $\sigma_2$ , respectively.

An example of the post-processing of a single numerical torque measurement is depicted in Figure 4.4.

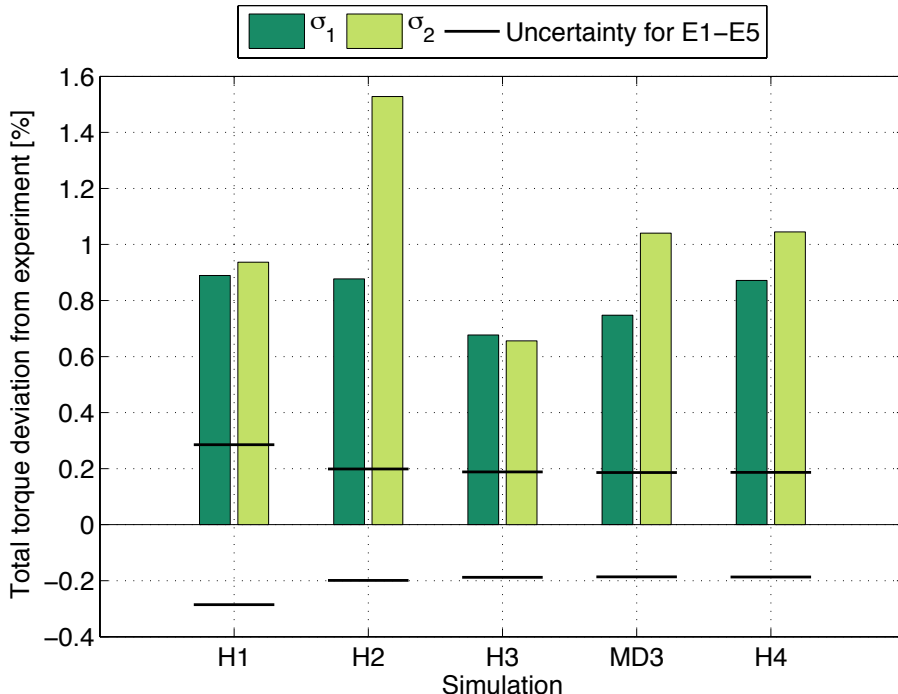


Figure 4.3: Total torque  $\tau_{tot}$  deviation between head simulations and experiments E1-E5.

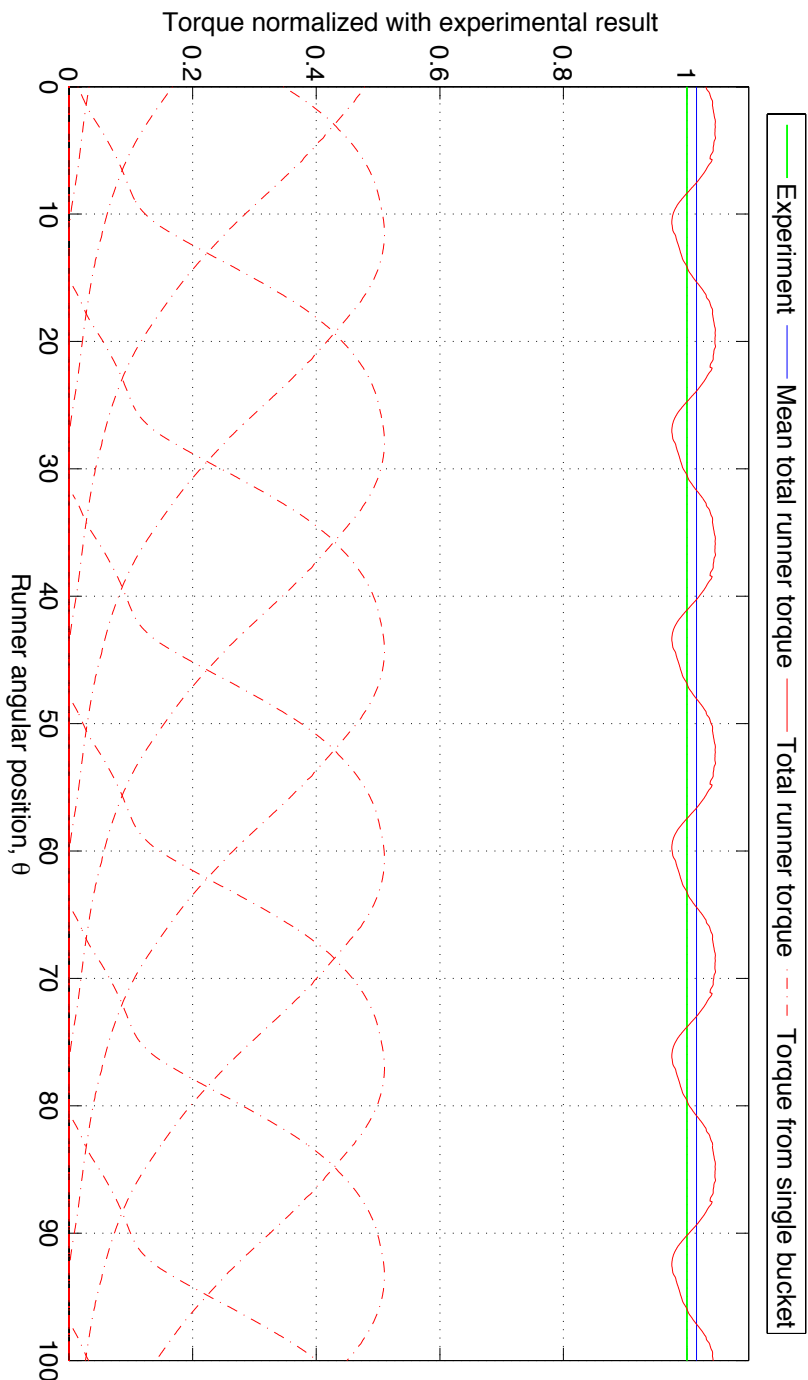


Figure 4.4: MD6 ( $\sigma_2$ ) simulation vs. experiment (E4)

## 4.3 Discussion

### 4.3.1 Uncertainty of Experimental Results

Errors were discovered in the calibration of the measurement instruments conducted by Aryal, Rajkarnikar and Adhikari. Therefore, Reinertsen's calibration from January 2012 was used to estimate the uncertainty of the experimental torque measurements. This is not an optimal solution, the calibration should have been performed right before and preferably after the experiments were conducted. Thus, the uncertainties calculated in this thesis are just approximations. They will, however, propose the general magnitude of the uncertainty. Reinertsen achieved an uncertainty of 0.2230% at 70m, which is only 0.035% higher than what the author achieved at 70m. This small deviation stems from the random errors in the measurement (Section B.1.2).

Later, a comparison of Aryal's and Reinertsen's generator torque calibration curves, showed that Aryal's curve aligned perfectly with Reinertsen's curve. At the same time, Aryal's uncertainty band was closer to the curve. Thus, the uncertainty for the generator torque used in this thesis can be considered valid. The friction torque calibration by Aryal, Rajkarnikar and Adhikari had failed, and was incomparable with Reinertsen's calibration. Given that the friction torque has such a small impact on total uncertainty, the total uncertainty calculated was considered adequate as an approximation.

### 4.3.2 Hydraulic Efficiency

For MD5-8,  $1 < \eta_{num}/\eta_{exp} < \tau_{num}/\tau_{exp}$ , where subscript *num* and *exp* represents numerical and experimental values, respectively. As expected,  $\eta_{num} > \eta_{exp}$ , probably due to the simplified CFD model.

The various operating parameters in the experiments were difficult to match the simulations. Therefore there are numerous parameters which either have a positive or negative effect on the efficiency. Generally, it is difficult to discuss the efficiency because the uncertainty of this value was not estimated.

### 4.3.3 Validity of the CFD Model

Compared to the *E4* experiment, the mesh dependency simulations are considered successful. The deviation between the numerical torque measurements and experimental torque measurements varies between 0.64 – 1.79 % and 0.32 – 1.62 % for  $\sigma_1$  and  $\sigma_2$ , respectively. For  $\sigma_2$ , the results show that one can expect the CFD model to over-predict the torque by approximately 1.5%. An over-prediction is indeed expected because the model does not account for various losses. These losses are

mainly the air resistance and back flow caused by presence of a turbine housing. If steady-state had been achieved, the air would contain small water droplets resulting in a bigger drag loss.

The head experiments show that the model is fairly independent of the head in the tested range of  $40m$  to  $80m$ . This conclusion is based on the fact that the variation in the deviation between the numerical and experimental torque measurements, is smaller than the uncertainty of the experiments. However, the gap between  $H2(\sigma_2)$  and the mean variation of the other simulations is a bit larger than the uncertainty. This may be a result of the use of a non-independent mesh (MD3). The uncertainty of the experiments may not be directly comparable to the uncertainty of the experiments, but it shows the magnitude of the discussed variation.

Based on the experimental results and numerical verification in the previous chapter, the CFD model is considered valid for its intended use, which is to predict the middle bucket torque. The author would like to stress that the torque prediction of  $+1.5\%$  only applies for the bucket geometry used in this thesis and the tested head range. For a geometry independent torque prediction, the model should be tested and validated for several different geometries. Furthermore, the model can only be considered valid for a head of  $75m$  because the mesh used in the head tests was smaller than the mesh independent size.

# Chapter 5

## Conclusion and Further Work

The CFD model presented in this thesis was found valid for it's intended use, which is to predict the torque applied to a Pelton bucket subject to a high-speed water jet. The validity, however, is restricted to the specific geometry used in this thesis and a head of  $75m$ . Under these conditions, the model over-predicts the torque by approximately 1.5%. An over-prediction was expected due to simplifications made in the model. A geometry independent torque prediction, requires a validation of several different geometries.

Mesh independency occurred at approximately  $4.5 \times 10^5$  elements. Head independence was also achieved in the tested range of  $40\text{-}80m$ , but may be questionable because the mesh size used in these simulations was below the mesh independent size.

As concluded by Klemetsen [3], surface tension has a small impact on the solution. However, the physical correct surface tension coefficient ( $\sigma$ ) gave a slightly more credible result in the mesh dependency test. Given that the model presented includes the surface tension coefficient, the physical correct value is recommended.

A natural extension of this thesis would be to validate the model for other bucket geometries. Soon, this may be possible at the Waterpower laboratory at NTNU, as doctoral candidate B. Solemslie is currently working on a Pelton bucket design. The production of a model runner based on this design may also be realized during the autumn of 2012. If the torque prediction is found to be constant for several geometries, a true validation is within reach. Then, the possibility of conducting parametric studies arise. Hence, the model may be used as a bucket design tool and be a part of the Pelton design software described in the introduction of this thesis.

Further improvements of the CFD model should focus on implementing a better nozzle approach and a jet velocity profile. Klemetsen's work showed that the adjustments made to the velocity profile, had the greatest impact on the results.

The stationary domain had varying mesh sizes throughout the simulations, which may have resulted in inconsistent torque measurements. Thus, the author recommends a single mesh size for the stationary domain.

In this thesis the experimental operational points did not match exactly with the numerical operational points. A perfect match is not possible due to the nature of the turbine regulation in the lab. A solution to this would be to run the simulations with the same operational conditions as the experiments. Then, the nozzle diameter  $d_s$  in the model would have to be adjusted in order to achieve the same volume flow measured experimentally. In the CFD model  $Q = c_1(\pi/4)d_s^2$  where  $c_1$  is bound by  $H_e$  ( $c_1 = (2gH_e)^{1/2}$ ). Using this method the error of the prediction could decrease.

A method for measuring  $y^+$  would also make the model more credible, as this is an important parameter in CFD simulations.

# Bibliography

- [1] Gotfred Severin Berntsen. *Numerical analysis of the two-phase Pelton jet flow using a single-phase model and analytical discussions of the Pelton jet surface break-up phenomenon*. PhD thesis, Department of Energy and Process Engineering, Norwegian University of Science and Technology, 2003.
- [2] Alexandre Perrig. *Hydrodynamics of the Free Surface Flow in Pelton Turbine Buckets*. PhD thesis, University of Lausanne, 2007.
- [3] Lars Erik Klemetsen. An experimental and numerical study of the free surface pelton bucket flow. MSc thesis, Norwegian University of Science and Technology, 2010.
- [4] IEC TC/SC 4. *IEC 60193 Ed. 2.0 b:1999, Hydraulic turbines, storage pumps and pump-turbines - Model acceptance tests*. Multiple. Distributed through American National Standards Institute (ANSI), August 2007.
- [5] Ole Gunnar Dahlhaug. Turbomachinery course (TEP4195), 2011.
- [6] Frank White. *Viscous fluid flow*. McGraw-Hill Higher Education, New York NY, 3rd ed. edition, 2006.
- [7] EDR. Introduction to ANSYS meshing v13, 2012.
- [8] ANSYS. *CFX Modeling/Theory Guide 13.0*, 2010.
- [9] Kyrre Reinertsen. Pelton model test rig at the waterpower laboratory, NTNU. MSc thesis, Norwegian University of Science and Technology, 2012.
- [10] Kristine Gjøsæter. Hydraulic design of francis turbine exposed to sediment erosion. MSc thesis, Norwegian University of Science and Technology, 2011.
- [11] Peter Joachim Gogstad. Hydraulic design of francis turbine exposed to sediment erosion. MSc thesis, Norwegian University of Science and Technology, 2012.
- [12] Hermod Brekke. Turbine design. In *State of the Art Turbine Design*, Beijing, China, September 2001.
- [13] Morten Hana. *Numerical analysis of non-stationary free surface flow in a Pelton bucket*. PhD thesis, Norwegian University of Science and Technology, Department of Thermal Energy and Hydropower, 1999.
- [14] DynaVec. <http://www.dynavec.no/>, December 2011.
- [15] Lorentz Fjellanger Barstad. *Pelton Model Test and Numerical Analysis*. Project thesis, Norwegian University of Science and Technology, December 2011.
- [16] Hermod Brekke. *Grunnkurs i Hydrauliske StrÅmningsmaskiner*. Vannkraftlaboratoriet NTNU, 2000.

- [17] Frank M. White. *Fluid mechanics*. McGraw-Hill, New York, 6th ed. edition, 2008.
- [18] Arne Kjølle. *Hydropower in Norway - Mechanical Equipment*. NTNU, 2001.
- [19] Maria Fernandino. Engineering fluid mechanics - specialization course (TEP4545), 2011.
- [20] Jørgen Tande. CDF study of a 10 MW offshore horizontal axis wind turbine blade. MSc thesis, Norwegian University of Science and Technology, 2011.
- [21] Martin Aasved Holst. *CFD analysis of wave induced loads on tidal turbine blades*. Project thesis, Norwegian University of Science and Technology, 2011.
- [22] F. R. Menter. Two-equation eddy-viscosity turbulence models for engineering applications. *AIAA Journal*, 32(8):1598–1605, August 1994.
- [23] David C Wilcox. Reassessment of the scale-determining equation for advanced turbulence models. *AIAA Journal*, 26(11):1299–1310, 1988.
- [24] Alexandre Perrig, Francois Avellan, Jean-Louis Kueny, Mohamed Farhat, and Etienne Parkinson. Flow in a pelton turbine bucket: Numerical and experimental investigations. *Journal of Fluids Engineering*, 128(2):350, 2006.
- [25] J E Bardina, P G Huang, and T J Coakley. Turbulence modeling validation, testing, and development. *Nasa Technical Memorandum*, (April), 1997.
- [26] B. Zoppe, C. Pellone, T. Maitre, and P. Leroy. Flow analysis inside a pelton turbine bucket. *Journal of Turbomachinery*, 128(3):500–511, July 2006.
- [27] H.B. Matthias and O. Promper. Numerical simulation of the free surface flow in pelton turbines. Timisoara, Romania, 2004.
- [28] Aiaa guide for the verification and validation of computational fluid dynamics simulations. Aiaa, [S.l.], 1998.
- [29] J.U Brackbill, D.B Kothe, and C Zemach. A continuum method for modeling surface tension. *Journal of Computational Physics*, 100(2):335–354, June 1992.
- [30] EDR Support. <http://www.edr.no/support>.
- [31] Hermod Brekke. *Pumper & Turbiner*. 2003.
- [32] Bjørn Winther Solemslie. Optimization of distribution system for a pelton turbine. MSc thesis, Norwegian University of Science and Technology, 2010.

# Appendices



# Appendix A

## CFD

The following sections are mainly derived from [6].

### A.1 Fundamental Equations

The governing equations of viscous flow are based on the three laws of conservation for physical systems:

1. Conservation of mass (continuity)
2. Conservation of momentum (Newton's second law)
3. Conservation of energy (first law of thermodynamics)

These laws are Lagrangian in nature, in other words, they apply to fixed systems (particles) that can be defined as a small fluid element and be adapted for use in fluid motion. Written on the non-conservative\* form they are, respectively,

$$\frac{\partial \rho}{\partial t} + \rho \nabla \cdot \mathbf{V} = 0 \quad (\text{A.1})$$

$$\rho \frac{D \mathbf{V}}{Dt} = \rho \mathbf{g} + \nabla \cdot \tau'_{ij} - \nabla p \quad (\text{A.2})$$

$$\rho \frac{D h}{Dt} = \frac{D p}{Dt} + \nabla \cdot (k \nabla T) + \Phi \quad (\text{A.3})$$

where  $\Phi$  denotes the dissipation function,  $\frac{D \mathbf{V}}{Dt} = \frac{\partial \mathbf{V}}{\partial t} + (\mathbf{V} \cdot \nabla) \mathbf{V}$  and the viscous stress tensor  $\tau'_{ij}$  for a newtonian fluid is:

---

\*The CFD-code ANSYS CFX use the conservative form of the fundamental equations.

$$\tau'_{ij} = \mu \left( \frac{\partial u_i}{\partial x_j} + \frac{\partial u_j}{\partial x_i} \right) + \delta_{ij} \lambda (\nabla \cdot \mathbf{V}) \quad (\text{A.4})$$

The scalar form of Eq. (A.2) is also known as the Navier-Stokes equations (x,y and z direction). The fluid flow that is going to be analyzed numerically in this thesis can be considered incompressible, i.e. the density  $\rho$  is constant. The continuity and momentum equation reduces to (A.5) and (A.6) respectively:

$$\nabla \cdot \mathbf{V} = 0 \quad (\text{A.5})$$

$$\rho \frac{D\mathbf{V}}{Dt} = \rho \mathbf{g} + \mu \nabla^2 \mathbf{V} - \nabla p \quad (\text{A.6})$$

The temperature effects of the flow will not be taken into account which mean that the energy equation (A.3) can be neglected.

## A.2 RANS Turbulence Modeling

The fluid is assumed to be in a randomly unsteady turbulent state, where any variable  $G$  is resolved into a mean value  $\bar{G}$  plus a fluctuating value  $G'$ . The mean value is, by definition,

$$\bar{G} = \frac{1}{T} \int_{t_0}^{t_0+T} G \, dt \quad (\text{A.7})$$

where  $T$  is large compared to the relevant period of fluctuations. As seen on Figure 2.5 the mean value  $\bar{G}$  may vary slowly with time (unsteady turbulent flow).

$$u = \bar{u} + u' \quad v = \bar{v} + v' \quad w = \bar{w} + w' \quad p = \bar{p} + p' \quad (\text{A.8})$$

$$\bar{u} = \overline{\bar{u} + u'} = \bar{u} + 0 \quad \Rightarrow \quad \bar{\bar{u}} = \bar{u} \quad (\text{A.9})$$

Inserting (A.8) into (A.6) and taking the time-average (A.9) of the velocity components  $u, v, w$  and pressure  $p$ , one obtain

$$\rho \frac{D\bar{\mathbf{V}}}{Dt} + \rho \frac{\partial}{\partial x_j} (\overline{u'_i u'_j}) = \rho \mathbf{g} + \mu \nabla^2 \bar{\mathbf{V}} - \nabla \bar{p} \quad (\text{A.10})$$

which is the incompressible vector form of the mean momentum equation. The new turbulent inertia tensor  $\overline{u'_i u'_j}$  has introduced nine new variables (tensor components). Rearranging this new tensor, Eq. (A.10) becomes

$$\rho \frac{D\bar{\mathbf{V}}}{Dt} = \rho \mathbf{g} + \nabla \cdot \tau_{ij} - \nabla \bar{p} \quad (\text{A.11})$$

where

$$\tau_{ij} = \underbrace{\mu \left( \frac{\partial u_i}{\partial x_j} + \frac{\partial u_j}{\partial x_i} \right)}_{\text{Laminar}} - \underbrace{\rho \overline{u'_i u'_j}}_{\text{Turbulent}}$$

and one recognizes that the turbulent inertia terms are displayed like they were stresses. Mathematically they behave as if the total stress on the system were composed by newtonian viscous stresses plus an additional turbulent-stress tensor  $-\rho \overline{u'_i u'_j}$  (6 new unknowns). The different turbulence models have different approaches to solving the RANS equations and is categorized by the number of new transport equations needed for closure (Table A.1).

Table A.1: RANS turbulence models sorted by number of extra transport equations needed for closure.

Transport Equations	Name
Zero	Mixing-length model
One	Turbulent kinetic energy
Two	K- $\epsilon$ model K- $\omega$ model SST model
Seven	Reynolds stress models



## Appendix B

# Uncertainty in Pelton Model Tests

This appendix describes the method used for calculating the uncertainties of the experimental torque measurements and is based mostly on [9] and [32].

## B.1 Torque

Note that each uncertainty in this section (B.1) must be calculated for both the generator torque and friction torque.

### B.1.1 Systematic Errors

Systematic errors  $e_s = f\tau_s \cdot \tau$  usually originate from a flaw in the equipment or in the design of the experiment. The systematic uncertainty of the torque measurement is related to the calibration of the torque transducer:

$$f\tau_s = f\tau_{cal} = \pm \sqrt{(f\tau_{reg})^2 + (f\tau_{arm})^2 + (f\tau_w)^2} \quad (\text{B.1})$$

where individual components are defined as

$f\tau_{reg}$  The uncertainty that arises from the regression process used to determine the calibration curve.

$f\tau_{arm}$  The systematic uncertainty related to the measuring of the length of the lever arm.

$f\tau_w$  The systematic uncertainty related to the weights used for calibration.

In this thesis Reinertsen's calibration data was used and the constant systematic uncertainties are presented in Table B.1. The Pelton logging systems automatically generates a data sheet containing the absolute error at different calibration points. These data points were used to create a calibration error curve  $y = e_{reg}(\tau)$  for the absolute uncertainty using a quadratic polynomial fitting. Then, the systematic uncertainty due to the regression process was calculated for specific heads (torque):

$$f\tau_{reg}(\tau) = \frac{e_{reg}(\tau)}{\tau}$$

Table B.1: Constant systematic uncertainties provided by Reinertsen. [9]

Torque type	$f\tau_{arm}$ [%]	$f\tau_w$ [%]
Generator, $\tau_{gen}$	0.00154	0.08536
Friction, $\tau_{fric}$	0.15	0.11

### B.1.2 Random Errors

Random errors are errors in the measurement system that lead to inconsistent output values when repeated measures of a constant input are taken. The uncertainty due to random errors in the measurement was calculated using a 95% confidence interval:

$$f\tau_r = \pm \frac{t_{\alpha/2} \cdot \frac{S_X}{\sqrt{N}}}{\tau} \quad (\text{B.2})$$

where  $t_{\alpha/2}$  is the Student-t value for confidence level  $1 - \alpha$  and  $N$  is the total number of samples.  $S_X$  is the standard deviation for the samples:

$$S_X = \sqrt{\frac{1}{N-1} \sum_{i=1}^N (x_i - \bar{X})^2} \quad (\text{B.3})$$

where  $x_i$  is the value of sample  $i$  and  $\bar{X}$  is the mean value of all samples in the measurement.

### B.1.3 Total Uncertainty

When the systematic and random errors are combined, the total uncertainty of the torque measurement becomes:

$$f\tau = \pm \sqrt{(f\tau_s)^2 + (f\tau_r)^2} \quad (\text{B.4})$$

## B.2 Total Torque

To calculate the total uncertainty for the generator torque and friction torque combined, the following uncertainties must first be calculated separately for both the generator torque and friction torque:  $f\tau_{reg}$ ,  $f\tau_{cal}$ ,  $f\tau_r$  and  $f\tau$ .

Finally, the total uncertainty of the torque measurement is

$$f\tau_{tot} = \pm \frac{\sqrt{(f\tau_{gen} \cdot \tau_{gen})^2 + (f\tau_{fr} \cdot \tau_{fr})^2}}{\tau_{gen} + \tau_{fr}} \quad (\text{B.5})$$

where  $\tau_{gen}$  and  $\tau_{fr}$  is the mean generator torque and friction torque in the measurements, respectively. Equation (B.5) is based on the absolute error, thus the magnitude of the generator torque and friction torque is taken into account. Hence, the relatively high uncertainty related to the friction torque does not have a high impact on the total uncertainty.



## Appendix C

# ANSYS DesignModeler Workflow

There are a couple of things to consider when one defines the fluid domain. The most important thing to remember, is to make sure that the jet is fully develop before the first bucket tip interacts with the jet. Because the angular velocity and jet velocity is known, this is easy to calculate. Another point to be made is that the symmetry plane should be the ZX-plane, and the fluid domain should lie on the positive side of the y-axis.

### C.1 Stationary domain

**Step 1** Create a new geometry component in Workbench and name it "Stationary". Enable "Named Selections" and set the "Named Selection Key" to blank. Open DesignModeler by double clicking the Geometry cell (green "DM" logo) in the "Stationary" component just created.

**Step 2** Create a new sketch in ZXPlane and name it "Stator". Create a drawing similar to the one shown on Figure C.1. Give it the appropriate dimensions. In this case,  $SR2 = SR1 \cdot 1.075$  and  $SA3 = 120^\circ$ .

**Step 3** Extrude the "Stator" sketch  $B$  mm in the positive y-direction where  $B$  is the bucket width on a complete bucket and set "Operation" to "Add Frozen".

**Step 4** Create a new plane and name it "NozzlePlane". Set "Type" to "From Plane" and "Base Plane" to "YZPlane". Offset the plane to the center of the nozzle outlet by specifying "Transform 1" and "Transform 2". To model a small part of the nozzle, increase the offset in the x-direction by approximately  $0.18 \cdot d_s$  where  $d_s$  is the water jet diameter.

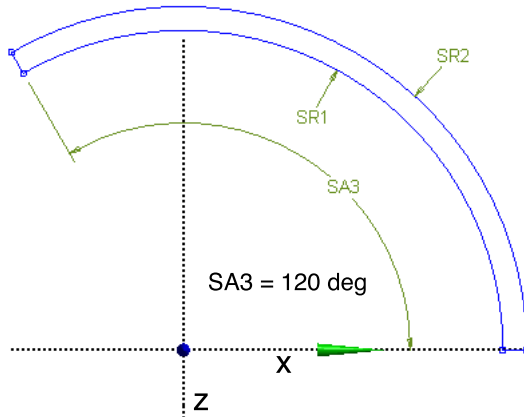


Figure C.1: Sketch: Stator

**Step 5** Create a new sketch in the plane "NozzlePlane" and name it "Nozzle1". Draw a half circle from the center of "NozzlePlane" and connect the ends by drawing a line. This sketch defines the outer walls of the jet domain. In this case  $NR1 = 1.55 \cdot d_s$ . See Figure C.2.

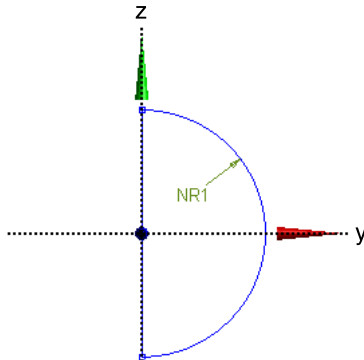


Figure C.2: Sketch: Nozzle1

**Step 6** Create a new sketch in the plane "NozzlePlane" and name it "Nozzle2". Draw two circles from the center of "NozzlePlane" as shown on Figure C.3. This sketch defines the solid nozzle wall. In this case  $ND3 - ND2 = 0.092 \cdot d_s$

**Step 7** Create two new sketches in the plane "NozzlePlane" and name them "JetSlice1" and "JetSlice2". In each sketch, draw a straight line from the center of "NozzlePlane" longer than the radius  $NR1$  on Figure C.2. In "JetSlice1" the line should point upwards and the line in "JetSlice2" should point downwards. Set the angle between the lines and the z-axis to  $45^\circ$ . See Figure C.4.

**Step 8** Create a new sketch in the plane "NozzlePlane" and name it "JetCore".

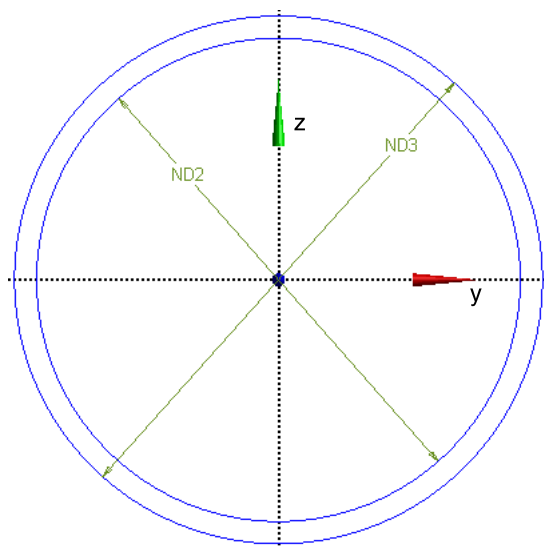


Figure C.3: Sketch: Nozzle2

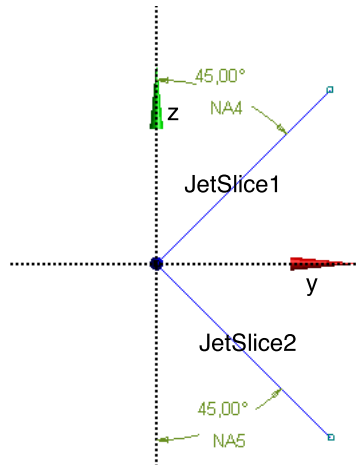


Figure C.4: Sketch: JetSlice1 and JetSlice2

Draw a square in the center of "NozzlePlane". In this case  $H8 = V7 = 0.5 \cdot H6 = 0.26 \cdot d_s$ . See Figure C.5.

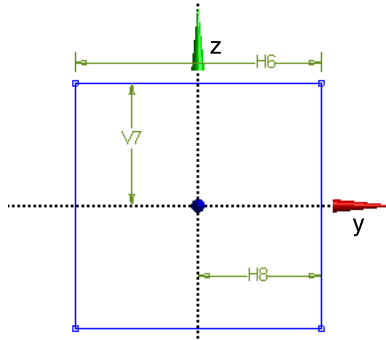


Figure C.5: Sketch: JetCore

**Step 8** Extrude the sketch "Nozzle1" in the direction of the part "Stator" created in Step 3 and set "Operation" to "Add Frozen". Set "Extent Type" to "To Surface" and select the outer face on the "Stator" as "Target Face".

**Step 9** Extrude the sketch "Nozzle2" in the direction of the part "Stator" created in Step 3 and set "Operation" to "Cut Material". Set "Extent Type" to "Fixed" and "Depth" to the length of the nozzle.

*In the Step 10 - 14 the nozzle domain will be sliced in several pieces in order to mesh the domain correctly.*

**Step 10** In Figure C.6 four surfaces are given the name S1-S4. These surfaces are going to be used to slice the nozzle domain in four operations. Start slicing (Create → Slice) the nozzle domain (light blue in Figure C.6) by the surface "S3". Set "Slice Type" to "Slice by Surface", select the surface "S3" as "Target Face" and select only the nozzle domain as "Slice Targets". For surface S1, S2 and S4, set "Slice Targets" to "All Bodies". The result of Step 10 is shown in Figure C.7. Note: all bodies must be frozen in order to use the Slice function.

**Step 11** The nozzle domain is now going to be sliced further, but now the extrude function will be used. Insert an Extrude and set "Base Object" to the sketch "JetSlice1", "Operation" to "Slice Material", "Extent Type" to "Through All", "As Thin/Surface?" to "Yes", "Inward Thickness" to "0 mm" and "Outward Thickness" to "0 mm". Select all bodies except the "Stator" part as "Target Bodies".

**Step 12** Repeat Step 11, but change "Base Object" to the sketch "JetSlice2".

**Step 13** It is optimal for the core of the water jet to be quadratical. Extrude the sketch "JetCore" in the same procedure as in "Step 11". Select all bodies that make up the water jet as "Target Bodies".

**Step 14** Now, the water jet core consists of 9 bodies. In this step this number will be reduced to 3 by "Unfreezing" and "Freezing". First, select the three upper

bodies (at the water inlet) of the core and insert an "Unfreeze" (Tools → Unfreeze). The selected parts are now merged into one body. Select this body and insert a "Freeze" (Tools → Freeze). Repeat this procedure two times going into the jet. The end result is shown in Figure C.8.

**Step 15** Select all bodies and form a new part called "Stationary" (RMB → Form New Part). The finished part should contain 28 bodies. Figure C.9 depicts the completed part "Stationary".

**Step 16** Create 6 "Named Selections" covering all free surfaces. In Figure C.9 all Named Selection are shown with their appropriate names.

**Step 17** Save the project and exit DesignModeler.

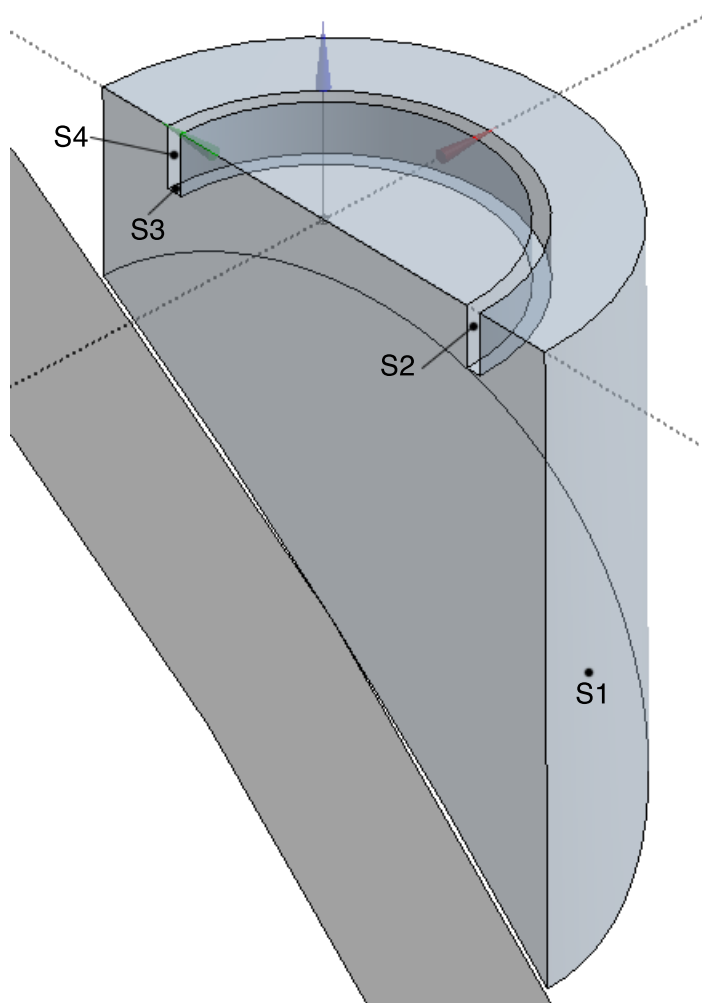


Figure C.6: Overview of the 4 slice surfaces in Step 10.

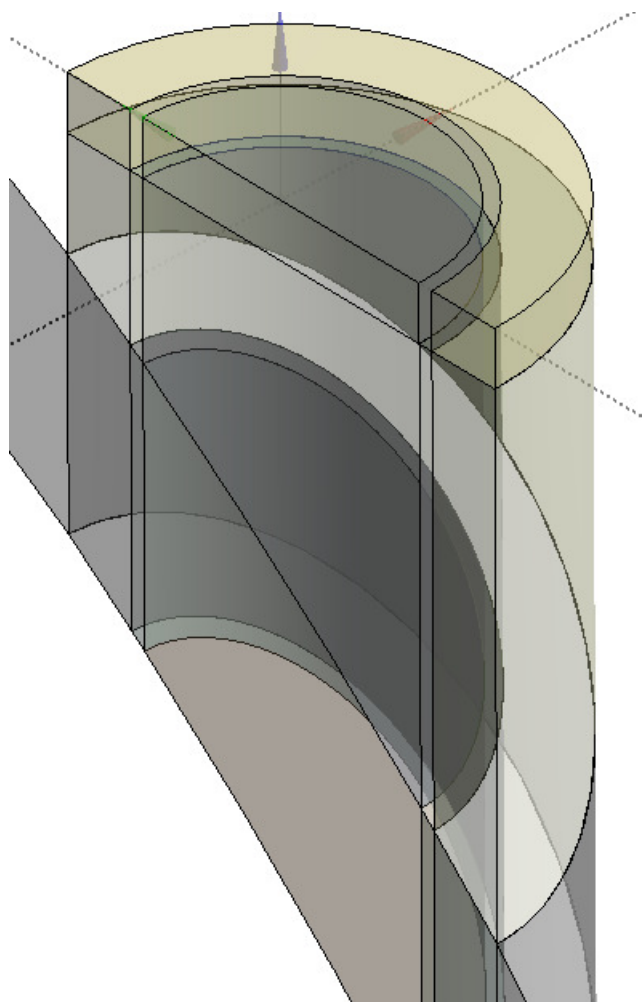


Figure C.7: Step 10 after slicing.

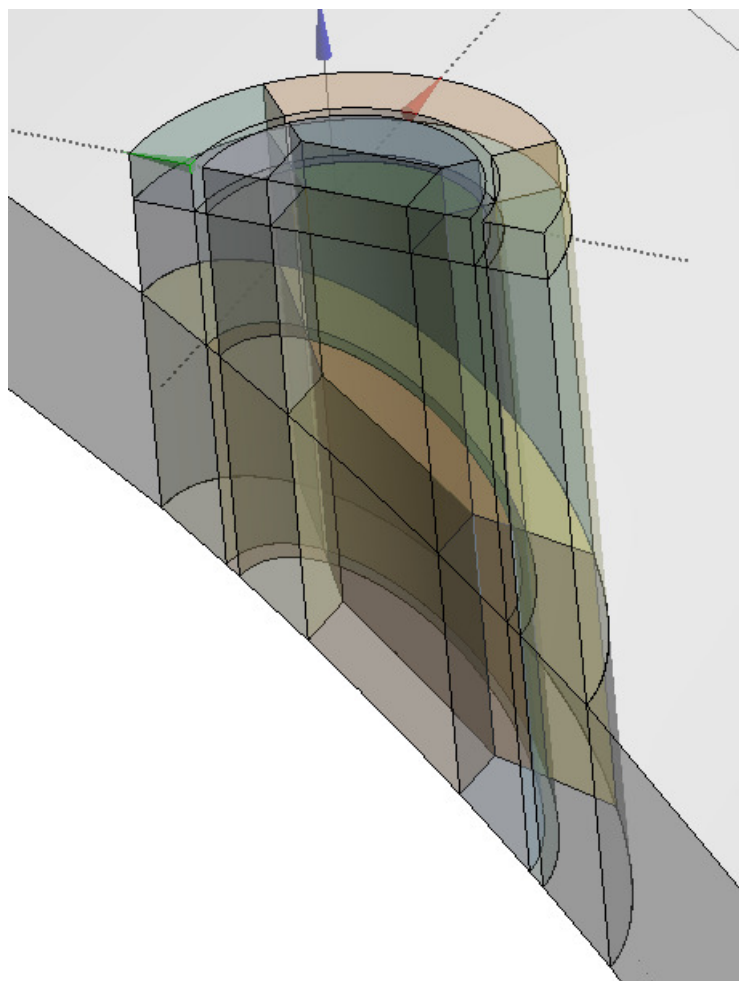


Figure C.8: Jet domain after slicing. Note that the jet core consists of three bodies.

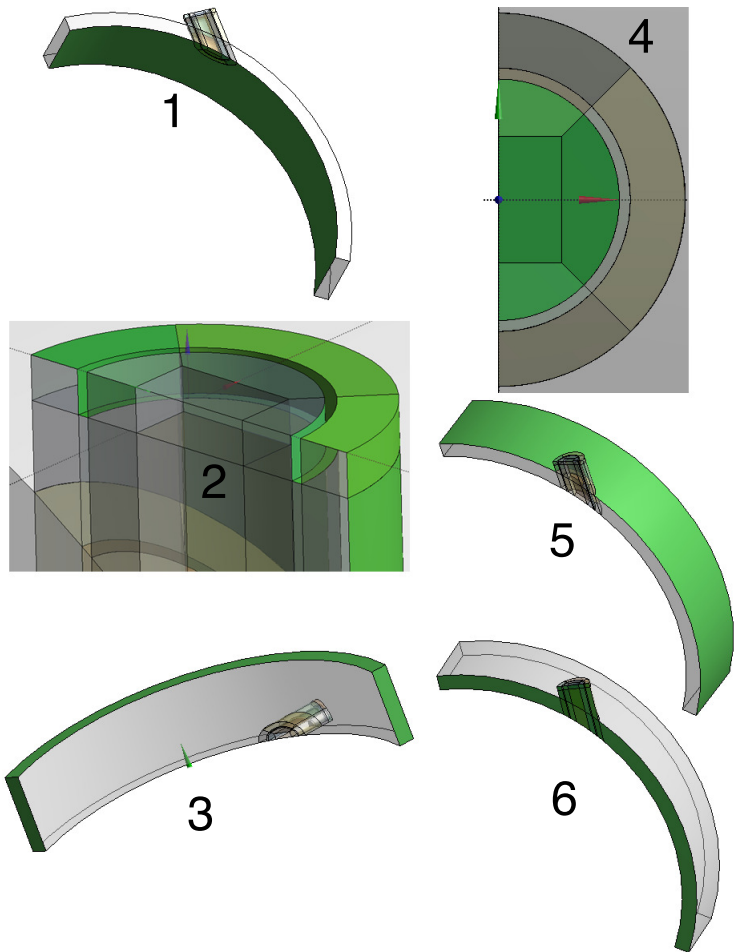


Figure C.9: Overview of the Named Selections (Green). (1) StatIF. (2) JetWalls. (3) StatOpening. (4) JetInlet. (5) StatInlet. (6) StatSym.

## C.2 Rotating domain

**Step 1** Create a new geometry component in Workbench and name it "Rotating". Enable "Named Selections" and set the "Named Selection Key" to blank. Open DesignModeler by double clicking the Geometry cell (green "DM" logo) in the "Rotating" component just created.

**Step 2** Import the bucket geometry (File → Import External Geometry File...) and set "Operation" to "Add Frozen".

**Step 3** If necessary, perform a "clean up" of the bucket geometry by merging or splitting appropriate faces. Useful tools are Merge (Tools → Merge), Edge Split (Concept → Split Edges) and Face Split (Tools → Face Split). Try to limit the number of sharp angles and faces to a minimum. This gives the elements a better quality and makes meshing easier on complex geometries.

**Step 4** Insert a new pattern (Create → Pattern) and set "Pattern Type" to "Circular". Select the imported bucket as "Geometry" and select the y-axis as "Axis". Set the "Angle" to  $(360 / \text{Total Number of Buckets on the Runner})$  and "Copies" to "2". Alter the copy direction by specifying a negative or positive angle. In this case a negative angle was used make two copies of the imported bucket in the positive angular direction about the y-axis. See Figure C.11.

**Step 5** Create a new sketch in the ZXPlane and name it "RotatingDomain". See Figure C.10.

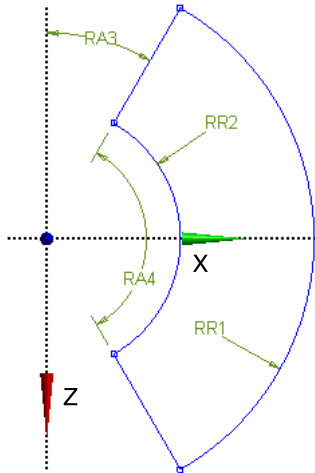


Figure C.10: Sketch: RotatingDomain.  $RA3 = 30^\circ$  and  $RA4 = 120^\circ$ .  $RR1 = SR1$  ( $SR1$  from Figure C.1).

**Step 6** Extrude the sketch "RotatingDomain"  $B$  mm in the positive y-direction where  $B$  is the bucket width on a complete bucket and set "Operation" to "Add

Frozen".

**Step 7** In this step the bucket bodies are going to be subtracted from the body created in Step 6 with a boolean operation. Insert a Boolean (Create → Boolean) and set "Operation" to "Subtract", select the "RotatingDomain" body as "Target Bodies" and select the three buckets as "Tool Bodies". Set "Preserve Tool Bodies?" to "No".

*In order to achieve a higher element density in the water jet region of interest, a method called "Body of Influence" will be used when meshing the rotating domain.*

**Step 8** Create a new sketch in the ZXPlane and name it "BoI1". Study Figure C.11. Draw two arcs using the "Arc by Center" tool and set the radius of RR5 and RR6 equal to RR2 and RR1 respectively. Connect the arcs by two splined lines using the "Spline" tool. Now it is up to the user to be creative when drawing the spline lines. In this thesis the goal was to achieve a high element density when the water jet is interacting with every bucket, but it maybe possible to reduce this area which will reduce the total number of elements and computational cost.

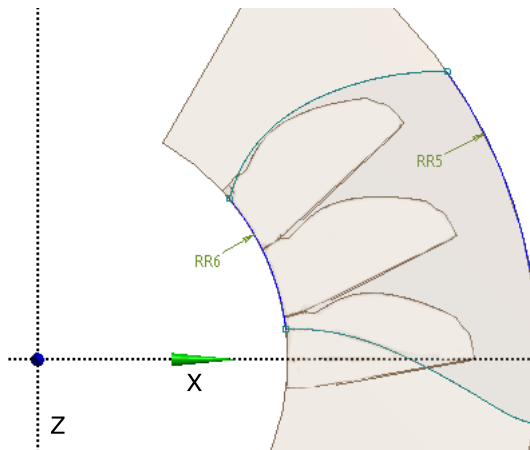


Figure C.11: Sketch: BoI1

**Step 9** Extrude the sketch "BoI1" in the positive y-direction. Set "Operation" to "Add Frozen", "Extent Type" to "Fixed" and the depth long enough to cover the GAP.

*A second body of influence was created at the outlet of the middle bucket to capture the flow in this area more accurately.*

**Step 10** Create a new plane on the rim of the middle bucket by setting "Type" to "From Face" and select the rim surface as "Base Face". Rotate the plane so that the plane normal matches the outlet angle. Create a sketch on this plane that cover the outlet area of interest, name it "BoI2" and extrude it to the next bucket by setting "Extent Type" to "To Faces" and specifying the target face.

To keep the number of elements at a minimum the Rotating domain is divided in two pieces ( $90^\circ$  and  $30^\circ$ ). It was decided that it was not necessary for the  $30^\circ$  piece to have the same element density as the  $90^\circ$  piece.

**Step 11** Create a new plane and set "Type" to "From Plane", select the XYPlane as "Base Plane", set "Transform 1" to "Rotate about Y" and "Value 1" to " $-30^\circ$ ".

**Step 12** Insert a Slice (Create → Slice) and set "Slice Type" to "Slice by Plane", select the plane created in Step 11 as "Base Plane" and select the rotating body as "Slice Targets".

**Step 13** Create "Named Selections" (NS) covering all free surfaces. For each bucket, create one NS for the entire bucket and one NS for the inside of the bucket (main flow region). The bucket named selections for the entire buckets are called TBC, MBC and BBC (Top, Middle, Bottom). The main flow regions are called TB, MB and BB. In Figure C.12 some of the Named Selection are depicted with their appropriate names.

**Step 14** Select the two bodies of influence and form a new part (RMB → Form New Part) and name it "Influence". Select the two remaining bodies and form a new part and name it "Rotating". The "Rotating" geometry component should now consist of two parts and four bodies.

**Step 15** Save the project and exit DesignModeler.

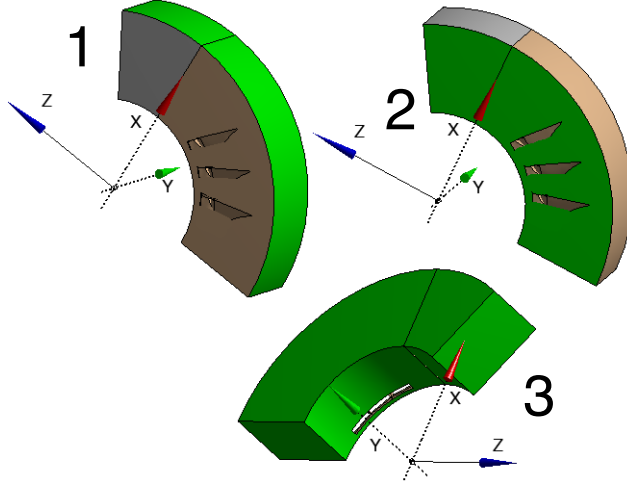


Figure C.12: Overview of the Named Selections (green face(s)) of the rotating domain. (1) RotIF. (2) RotSym. (3) RotOpen.

## Appendix D

# ANSYS Meshing Workflow

When working with ANSYS Meshing 13.0, one should be aware of that the order one applies sizings, inflations etc. has an impact on the success of mesh generation. It can be useful to temporarily suppress parts you are not working on to speed up mesh generation and avoid conflicts. The parameters used in this guide are only suggestions and experimenting with these parameters will give a desired number of elements.

### D.1 Stationary domain

**Step 1** Create a new mesh component in Workbench and name it "Stationary mesh". Connect the geometry from the geometry component "Stationary" created in Appendix C to the mesh component just created. Double click the "Mesh" cell to open ANSYS Meshing.

**Step 2** Hide the upper layer of bodies of the jet domain as shown in Figure D.1. In Figure D.1a the surfaceses have been given digit names. Example: Area "A2" corresponds to the multiple selection of every area/surface named "2". Body "B2" is the multiple selection of every body named "2".

*It is important to update/generate the mesh between every step from now on to make sure that each setting works properly. Errors are also easier to identify by updating the mesh often.*

**Step 3** Insert a Face Sizing and select "A1" as "Geometry", set "Type" to "Element Size" and specify an element size of 1mm.

**Step 3** Insert a Face Sizing and select "A2" as "Geometry", set "Type" to "Element Size" and specify an element size of 1mm.

**Step 4** Insert a Sweep Method and select "B1" as "Geometry", set "Method"

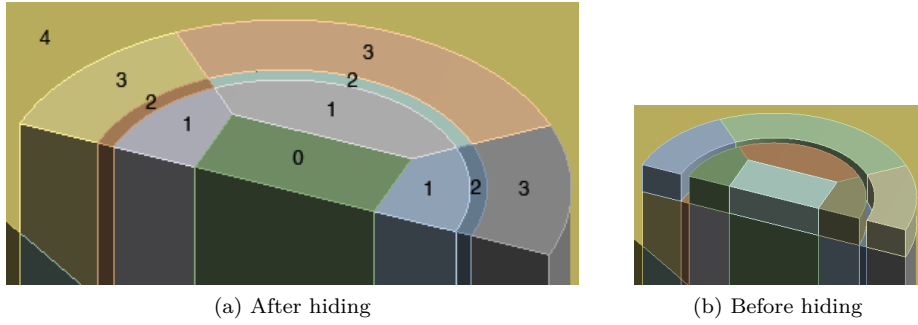


Figure D.1: Area numbering

to "Sweep", "Src/Trg Selection" to "Manual Source and Target", select "A1" as "Source", select the bottom faces of "B1" as "Target", set "Type" to "Number of Divisions" and "Sweep Num Divs" to "20". The mesh pattern of "A1" is now swept through "B1" in the flow direction.

**Step 5** Repeat Step 4 for "A2" and "A3".

**Step 6** Insert an Inflation and select "A1" as "Geometry". Select the three edges on the air-water interface as "Boundary", set "Inflation Option" to "First Layer Thickness", "First Layer Height" to 0.1mm and "Maximum Layers" to "10".

**Step 7** Repeat Step 6 for "A2". Note that the air-water interface is still the boundary.

**Step 8** Insert a Face Sizing and select "A3" as "Geometry", set "Type" to "Element Size" and specify an element size of 2mm.

**Step 9** Unhide the bodies hidden in Step 2. Insert a Sweep Method and select the bodies hidden in Step 2 as "Geometry" (7 bodies in total). Set "Method" to "Sweep", "Src/Trg Selection" to "Manual Source and Target", select "A0+A1+A3" as "Source", select the top faces of "A0+A1+A3" as "Target", set "Type" to "Number of Divisions" and "Sweep Num Divs" to "5".

**Step 10** Insert a Body Sizing and select "B4" as "Geometry". Set "Type" to "Element Size" and specify an element size of 4mm.

**Step 11** Hide "B0", "B1", "B2" and "B3". Insert a Sweep Method and select all the lower bodies of the jet domain as "Geometry" (10 bodies in total). Set "Method" to "Sweep", "Src/Trg Selection" to "Manual Source and Target", select all faces closest to the water inlet (10 faces) as "Source", select the bottom faces of the jet domain (10 faces) as "Target", set "Type" to "Number of Divisions" and "Sweep Num Divs" to "15".

**Step 12** Save the project and close Meshing.

## D.2 Rotating domain

**Step 1** Create a new mesh component in Workbench and name it "Rotating mesh". Connect the geometry from the geometry component "Rotating" created in Appendix C to the mesh component just created. Double click the "Mesh" cell to open ANSYS Meshing.

**Step 2** Insert a Body Sizing and select "RB1" as "Geometry". Set "Type" to "Body of Influence", select the body "BoI1" as "Bodies of Influence" and specify an element size of 2mm.

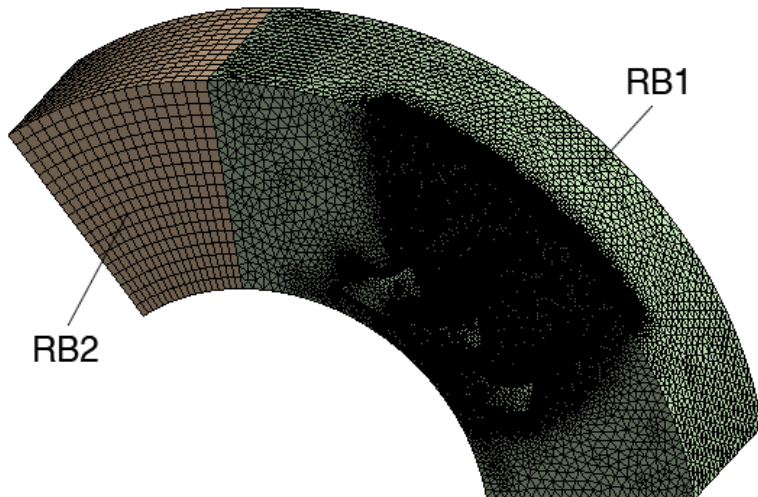


Figure D.2: Rotating mesh

**Step 3** Insert a Body Sizing and select "RB1" as "Geometry". Set "Type" to "Body of Influence", select the body "BoI2" as "Bodies of Influence" and specify an element size of 2mm.

**Step 4** Insert an Inflation and "RB1" as "Geometry". Set "Boundary Scoping Method" to "Named Selections", select "MB" as "Boundary", set "Inflation Option" to "First Layer Thickness", "First Layer Height" to 0.1mm and "Maximum Layers" to "10".

**Step 5** Insert a Face Sizing, set "Scoping Method" to "Named Selection", select "MB" as "Named Selection", "Type" to "Element Size" and specify an element size of 0.8mm.

**Step 6** Repeat Step 4 for "TB".

**Step 7** Insert a Body Sizing and select "RB1" as "Geometry". Set "Type" to "Element Size" and specify an element size of 8mm.

**Step 8** Insert a Body Sizing and select "RB2" as "Geometry". Set "Type" to Element Size" and specify an element size of  $10mm$ .

**Step 9** Sweep "RB2" in the rotational direction by specifying a Face Sizing of  $8mm$  on the interface of "RB1" and "RB2".

**Step 10** Save the project and close Meshing.

## Appendix E

# ANSYS Pre Detailed Setup

The CFD analysis with the CFX solver is created by connecting the rotating and stationary mesh to a CFX component. By double clicking the "Setup" in the CFX component ANSYS Pre is launched. The natural workflow in ANSYS Pre is to start at the top of the "Outline" tree and work your way down. Every option that is not mentioned here were left at the default setting. A lot of the settings here use named selections created in Appendix C.

### E.1 Expressions

Create the expressions listed in table E.1. Defining expressions is a good way of streamlining a CFD case. In the head dependency tests, the head was changed very easily by adjusting the constant "Head". Then, the value of expressions depending on the head automatically changes.

When a constant like the head is defined, one simply defines the unit with brackets. For example, the head expression becomes  $75 [m]$ . The turbine radius is defined in millimeters, but ANSYS recognizes this and is able to convert the units automatically when for instance  $[m]$  and  $[mm]$  are used in the same expression.

Table E.1: Expressions defined in ANSYS Pre

Name	Expression	Description
Gravity	9.82 [m s <sup>-2</sup> ]	Acceleration of Gravity
Head	75 [m]	Head
TurbRad	x [mm]	Turbine radius
InletVel	(2*Gravity*Head) <sup>0.5</sup>	Absolute water velocity at the nozzle inlet
Omega	InletVel / (2*TurbRad)	Angular velocity. Optimal peripheral velocity is $0.5 \cdot InletVel$
TorqueMBC	torque_y@REGION:MBC	Total torque on the middle bucket. "MBC" is the named selection for the entire middle bucket.
TotalTime	((120*pi) / 180) / Omega	Total simulation running time
DataStep	TotalTime / 10	Timestep for data logging

## E.2 Analysis Type

- Analysis Type = Transient
- Time Duration = Total Time = TotalTime (expression)
- Time Steps = Adaptive
- First Update Time = 0.0 [s]. Timestep Update Freq. = 1. Initial Timestep = 0.0001 [s].
- Timestep Adaption: Option = Num. Coeff. Loops. Maximum Timestep = 0.0003 [s]. Minimum Timestep = 0.00001 [s]. Target Max. Loops = 8. Target Min. Loops = 4. Timestep Decrease Fac = 0.8. Timestep Increase Fac = 1.06.
- Initial Time = Automatic with Value = 0 [s].

## E.3 Domains

Start by deleting the automatically created default domain. Insert two new domains and name them "Rotating" and "Stationary".

**Basic Settings tab for both domains**

- Define fluid properties for both air and water.
- Reference Pressure: 1 [atm].
- Domain Type: Fluid Domain

#### **Basic Settings tab for rotating domain**

- Set Domain Motion to Rotating with the Angular Velocity defined by the expression "Omega".
- Rotation Axis: Global Y.

#### **Basic Settings tab for stationary domain**

- Domain Motion: Stationary

#### **Fluid Models tab for both domains**

- Enable the Homogeneous Model.
- Select the Standard Free Surface Model.
- Select the Shear Stress Transport turbulence model with the automatic wall function.
- There is no heat transfer, combustion or thermal radiation in this CFD model.

#### **Fluid Pair Models tab for both domains**

- Enable the "Surface Tension Coefficient" for the air-water pairing and set it to 0.7 [ $\text{N m}^{-1}$ ].
- Select the "Continuum Surface Force" surface tension model option with the primary fluid set to Water.

#### **Initialization tab for both domains**

- Enable the Domain Initialization.
- Set Velocity Type to Cartesian and set U,V and W to 0 [ $\text{m s}^{-1}$ ].
- Relative Pressure: 0 [Pa]
- Set the initial volume fraction for air and water to 1 and 0 respectively.

## **E.4 Boundary Conditions**

#### **Boundary conditions for the rotating domain**

- **Buckets:** Boundary Type = Wall. Location = BBC,MBC,TBC. Frame Type = Rotating. Mass And Momentum = No Slip Wall. Wall Roughness = Smooth Wall.

- **RotOpen:** Boundary Type = Opening. Location = RotOpen. Frame Type = Rotating. Flow Regime = Subsonic. Mass And Momentum = Opening Pres. and Dirn (Relative Pressure = 0 [Pa]). Air Volume Fraction = 1. Water Volume Fraction = 0.
- **RotSym:** Boundary Type = Symmetry. Location = RotSym.

### Boundary conditions for the stationary domain

- **JetInlet:** Boundary Type = Inlet. Location = JetInlet. Mass And Momentum = Normal Speed = InletVel. Air Volume Fraction = 0. Water Volume Fraction = 1.
- **JetWall:** Boundary Type = Wall. Location = JetWall. Mass And Momentum = No Slip Wall. Wall Roughness = Smooth Wall.
- **StatInlet:** Boundary Type = Inlet. Location = StatInlet. Mass And Momentum = Normal Speed = 0.1 [m s<sup>-1</sup>]. Air Volume Fraction = 1. Water Volume Fraction = 0.
- **StatOpen:** Boundary Type = Opening. Location = StatOpen. Flow Regime = Subsonic. Mass And Momentum = Opening Pres. and Dirn (Relative Pressure = 0 [Pa]). Air Volume Fraction = 1. Water Volume Fraction = 0.
- **StatSym:** Boundary Type = Symmetry. Location = StatSym.

## E.5 Interfaces

Delete the default interface, insert a new interface and name it "RSIF". The boundary conditions for the interfaces are created automatically ("RSIF Side 1" and "RSIF Side 2").

### Settings for the interface "RSIF"

- Interface Type = Fluid Fluid
- Interface Side 1: Domain (Filter) = Rotating. Region List = RotIF.
- Interface Side 2: Domain (Filter) = Stationary. Region List = StatIF.
- Interface Models = General Connection. Frame Change/Mixing Model = Transient Rotor Stator. Pitch Change = Value. Pitch Ratio = 1.

## E.6 Solver

### E.6.1 Solver Units

Mass Units = [kg]. Length Units = [m]. Time Units = [s]. Temperature Units = [K]. Angle Units = [rad]. Solid Angle Units = [sr].

### E.6.2 Solver Control

#### Basic Settings tab

- Advection Scheme = High Resolution
- Transient Scheme = Second Order Backward Upwind. Timestep Initialization = Automatic.
- Turbulence Numerics = First Order.
- Convergence Control: Min Coeff. Loops = 3. Max. Coeff. Loops = 10. Timescale Control = Coefficient Loops.
- Convergence Criteria: Residual Type = RMS. Residual Target = 0.000115.

### E.6.3 Output Control

#### Trn Results tab

- Create a new Transient Results item.
- Output Frequency = Time Interval = DataStep (expression)

#### Monitor tab

- Enable Monitor Objects
- Monitor Points and Expressions: Add a new monitor and name it "Torque\_MBC".
- Click on "Torque\_MBC", set Option to Expression and Expression Value to TorqueMBC (expression).



## Appendix F

# MATLAB Post-Processing

In this Section F.1 a short explanation of the CreateT.m script found in Section F.2 is presented.

### F.1 Total Torque Matrix

Using a while loop, different timesteps are tested and returns if the error in percent of the timestep  $\Delta t$

$$e = \frac{\left| \frac{1}{f_Z} - \left\| \frac{\frac{1}{f_Z}}{\Delta t} \right\| \cdot \Delta t \right|}{\Delta t} \quad (\text{F.1})$$

is smaller than a specified target, where  $\|x\|$  is the nearest integer to  $x$  and  $f_Z$  is the bucket frequency. Then the torque is calculated on the new timeline using a spline function.

Finally,  $n + 1$  identical torque series of  $k$  torque values, are combined in a single matrix  $T_{i,j}$ , containing time  $t$  in column 1, the original torque series in column 2 ( $n = 0$ ) and the  $n$  duplicated torque series  $T(k)$  in column 3 →  $n + 2$  and the total torque in column  $n + 3$ :

$$T_{i,j} = \begin{bmatrix} t_1 & T(1) & 0 & \dots & \sum_{j=2}^{n+2} T_{1j} \\ \vdots & \vdots & \vdots & \dots & \vdots \\ \vdots & \vdots & 0 & \dots & \vdots \\ t = 1 \cdot \frac{1}{f_z} & \vdots & T(1) & \dots & \vdots \\ \vdots & \vdots & \vdots & \dots & \vdots \\ \vdots & T(k) & \vdots & \dots & \vdots \\ \vdots & 0 & \vdots & \dots & \vdots \\ \vdots & \vdots & \vdots & \dots & \vdots \\ \vdots & \vdots & T(k) & \dots & \vdots \\ \vdots & \vdots & 0 & \dots & \vdots \\ \vdots & \vdots & \vdots & \dots & \vdots \\ t_i & 0 & 0 & \dots & \sum_{j=2}^{n+2} T_{ij} \end{bmatrix}$$

As shown in the matrix above, each duplicated torque series in column  $n + 2$  is shifted  $n \cdot \frac{1}{f_z}$  [s] downwards. Figure 3.5 is an example of the torque curves  $T_{(1 \rightarrow i), (2 \rightarrow n+2)}$  and the total torque  $T_{(1 \rightarrow i), (n+3)}$  plotted against the time  $T_{(1 \rightarrow i), 1}$ .

## F.2 File: CreateT.m

```
%----- CREATE TOTAL TORQUE MATRIX T -----
%
% The following code calculates a fixed timestep size and a matrix T
% containing 'nt' number of torque curves where each curve is shifted
% 'n*dt' in time. n is the number of duplicated torque curves. The sum
% of the torque is located in column 'n+3'. The 'target' variable is
% the maximum error in percent of the timestep size between 'dt' and
% shift*timestep'. 'shift' is number of timesteps in 'dt' found by
% rounding 'dt/timestep'. This rounding produces the error.
%
%----- INPUT -----
source = MD6;           %Source: torque in column 2 and time in column 3
target = 0.001;          %Error target [%]
nt = 10;                %Number of torque curves (n+1)
g = 9.82;               %Gravity
r = 250;                %Runner radius [mm]
Z = 22;                 %Number of buckets
H = 75;                 %Head [m]
%
%----- INPUT - END -----
c1 = sqrt(2*g*H);       %Bucket inlet velocity
omega = (c1/(2*r))*1000; %Angular velocity [rad/s]
fz = (omega*Z)/(2*pi);   %Bucket frequency [1/s]
dt = 1/fz;               %Bucket period [s]

%Create temporary torque matrix including (t,T) = (time,torque) = (0,0)
T_temp(1,1) = 0;
T_temp(2:size(source,1)+1,1) = source(:,3);
T_temp(1,2) = 0;
T_temp(2:size(source,1)+1,2) = source(:,2);
clear source

%Find minimum timestep in T_temp
for i = 2:size(T_temp(:,1),1)

    T_temp(i,3) = T_temp(i,1)-T_temp(i-1,1);

end
min_step = min(T_temp(2:end,3));

%Total time
t_tot = T_temp(end,1);

%Initial values for timestep iteration
error = 1;
timestep = 1;
i = size(T_temp(:,1),1);

%Find a timestep that meets the required target
while error >= target

    timestep = t_tot/i;
```

```

%Number of timesteps in one period
shift = round(dt/timestep);

%Error
error = abs((dt-timestep*shift)/timestep);
%error = abs((dt-timestep*shift)/dt);

if timestep > 0.5*min_step
    error = 1;
end

if error ≥ target
    i = i + 1;
else
    break
end

end

%Create timeline in torque matrix T
T(:,1) = 0:timestep:(t_tot+(nt*dt));

%Create spline of the original torque source
Ts(:,1) = 0:timestep:T_temp(end,1);
Ts(:,2) = spline(T_temp(:,1),T_temp(:,2),Ts(:,1));

%Insert the torque series in T matrix
L = size(Ts,1);
for k = 1:nt

    if k == 1
        T(1:L,k+1) = Ts(:,2);
    else
        T(shift*(k-1):shift*(k-1)+L-1,k+1) = Ts(:,2);
    end

end

%Create total torque sum in column n+3
p = find(T(:,k+1)≠0);
p = p(end); %Last row number in T matrix

for g = 1:p

    T(g,k+2) = sum(T(g,2:k+1));

end

%Delete all rows (empty) below row p
T(p+1:size(T,1),:) = [];

%Delete unwanted variables from the workspace
clear Ts k nt p L g T_temp

%----- END -----

```